Renormalization group approach to the onset of SNA in maps with the golden-mean quasiperiodic driving

August 20, 2004

1 Introduction: The main idea of the renormalization group analysis

Originally, the approach called *renormalization group analysis* (RG) was developed in the quantum field theory and in the phase transition theory [Shirkov *et al* (1988)], [Balescu (1975)]. Generally speaking, this is a tool to deal with objects possessing a wide interval of temporal and/or spatial characteristic scales.

In nonlinear dynamics the RG approach was introduced by Feigenbaum [Feigenbaum (1979)], [Feigenbaum (1983)] and latter applied successively for analysis of different types of transitions to chaos, e.g. via period doubling [Vul *et al.* (1984], [Cvitanović (1989)], [Kuznetsov *et al.* (1997)], intermittency [Hirsch *et al.* (1982)], [Hu and Rudnick (1982)], quasiperiodicity [Feigenbaum *et al.* (1982)], [Ostlund *et al.* (1983)]. As commonly recognized, this is an effective and powerful theoretical instrument uncovering deep and fundamental features of dynamics between order and chaos, like quantitative universality and scale invariance (scaling) for those subtle structures in phase space and in parameter space, which are associated with the transitions.

To explain the general idea of the RG method in the context of nonlinear dynamics, let us assume that we have an evolution operator for some dynamical system on a definite time interval. Applying this operator several times, we construct an evolution operator for a larger interval. An opportunity to

use the RG analysis occurs in a rather specific, so-called *critical situation*, when it is possible to adjust parameters of the original system in such way that the new operator for larger time interval can be transformed exactly or approximately to the initial operator by a change of scales of dynamical variable (variables). This procedure is called *an RG transformation*, and the adjusted parameters define location of the *critical point* in the parameter space of the original system. The RG transformation may be applied repeatedly to obtain a sequence of the evolution operators for larger and larger time scales.

A critical situation usually corresponds to convergence of the operator sequence to some definite limit, *a fixed point of the RG transformation*, or, as alternative, to *a periodic point* called also *a cycle*. However, the last possibility is not conceptually different, because in the case of period p one can speak of a fixed point of the RG transformation composed of p steps of the original construction.

Presence of a fixed point of the RG transformation means that the rescaled long-time evolution operators at the criticality will be of a universal form, up to a characteristic scale. In principle, this form of the renormalized operator may be recovered (say, numerically) directly from the operator fixed-point equation. The last is determined entirely by a structure of the RG scheme, i.e., without any reference to the originally examined system. Therefore, we assert that a fixed-point solution of a definite RG scheme gives rise to a *universality class*, which may include systems of very different mathematical nature (e.g. iterative maps, ordinary differential equations, extended systems, etc.)

What are dynamical consequences of the fact of convergence to the fixed point of the rescaled operators produced by application of the RG procedure? Obviously, this convergence means that at the critical point dynamics of the original system on different time scales are similar, up to the scale change of dynamical variables. This is a property called *scaling*.

Moreover, scaling regularities are intrinsic also to a vicinity of the critical point in the parameter space. Let us suppose that we depart a little from the critical point, and the system demonstrates some kind of dynamical behavior. Then, we can decrease the displacement in such way that the evolution operator after a larger number of steps of the RG transformation will be similar to that relating to the previous case. Therefore, we will have similar dynamics in the system, but with a larger characteristic time scale, and with smaller scales for the dynamical variables. As follows, a vicinity of

the critical point in the parameter space contains a self-similar configuration of domains, which is of common structure for the entire universality class. (In fact, the scaling property appears as asymptotic: the smaller is a vicinity of the critical point, the higher is accuracy of the observed self-similarity. In finite scales it may be regarded rather as approximation.)

As we speak about a vicinity of a critical point, we must examine small perturbations of the evolution operators near the fixed point of the RG transformation caused by detuning parameters from the critical situation. Under assumption of smallness of the perturbations, it may be done in terms of linear stability analysis for this fixed point of the RG transformation. It gives rise to some eigenvalue problem. Relevant eigenvalues in the spectrum are those, which are larger than 1 in modulus (that means, the perturbation grows under repetitive RG transformation). These eigenvalues play a role of *scaling factors* along appropriate axes in the parameter space. A number of relevant eigenvalues define a *codimension* of the critical situation; this is a number of parameters adjusted to reach the criticality. For instance, in a three-dimensional parameter space critical situations of codimension-one will occur at some surfaces, codimension-two at curves, and codimension-three at some points.

In respect of the solution of the RG equation, relevant eigenvalues are associated with *an unstable manifold*, along which the orbits depart from the fixed point under application of the RG transformation. Irrelevant eigenvalues, which are less in modulus then 1, correspond to *a stable manifold* and respond for the approach of the solutions to the fixed point, as the conditions of criticality are valid. It is clear from the present discussion, that for any type of critical behavior a fixed point of RG transformation must be of *saddle type*.

As argued in previous chapters, in quasiperiodically forced systems occurrence of SNA is a typical attribute of dynamics between order and chaos. Therefore, it is natural to expect that RG analysis may be relevant for understanding nature of SNAs, mechanisms of their birth, and, perhaps, for fundamental quantitative regularities intrinsic to these phenomena. Originally, we advanced this idea in a note [Kuznetsov *et al.* (1995)], devoted to the birth of SNA in the pitchfork bifurcation model under quasiperiodic force (called later the "blowout" transition [Yalçynkaya and Lai (1996)]). Then, we applied it to several types of critical points in parameter space of quasiperiodically driven maps (torus doubling terminal [Kuznetsov *et al.* (1998)], torus collision terminal [Kuznetsov *et al.* (2000)], and torus fractalization

[Kuznetsov (2002)]. Up to now, only a case of the golden mean quasiperiodic force was studied in a frame of this approach. Here we present a review of these results and discuss possible directions of further developments.

2 The basic functional equations for the golden-mean renormalization scheme

Let us consider a concrete formulation of the RG approach, appropriate to the quasiperiodically forced dynamics with the golden-mean frequency ratio and start with the basic model of a forced one-dimensional discrete-time system

$$x_{n+1} = f(x_n, u_n),\ u_{n+1} = u_n + w\,(\mathrm{mod}1), \tag{1}$$

where $w = (\sqrt{5}-1)/2$. This irrational value is approximated by ratios of subsequent Fibonacci numbers F_m, so, in construction of the RG scheme it is natural to consider evolution operators for the Fibonacci numbers of steps. Let the evolution operator over F_m steps be

$$x_{n+F_m} = f_m(x_n, u_n),\ u_{n+F_m} = u_n + F_m\, w\,(\mathrm{mod}1). \tag{2}$$

In accordance with definition of the Fibonacci numbers, $F_{m+2} = F_{m+1} + F_m$. Therefore, subsequent application of the evolution operators over F_{m+1} steps and then over F_m steps yields

$$x_{n+F_{m+2}} = f_m(f_{m+1}(x_n,\, u_n),\ \ u_n + wF_{m+1}). \tag{3}$$

To have a reasonable limit behavior of the sequence of evolution operators, we will change scales for x and u at each new step of the construction by appropriate factors α and β. One of the relations associated with the golden mean reads

$$F_{m+1} = -(-w)^{m+1}(\mathrm{mod}1). \tag{4}$$

As follows, the second rescaling factor definitely is $\beta = -1/w = -1.618034....$ Now, instead of f_m, we introduce the renormalized functions

$$g_m(x,u) = \alpha^m f_m(x/\alpha^m,\, (-w)^m u). \tag{5}$$

Rewriting (3) in terms of these functions we come to our RG equation [Kuznetsov *et al.* (1998)], [Kuznetsov *et al.* (2000)], [Kuznetsov (2002)], [Kuznetsov (2003)]

$$g_{m+2}(x,u) = \alpha^2 g_m(\alpha^{-1} g_{m+1}(x/\alpha,\, -uw),\, w^2u + w). \tag{6}$$

In a particular case, when the functions g_m do not depend on the second argument, this functional equation reduces to the equation derived earlier to describe critical behavior in an autonomous circle map at the golden-mean rotation number. It is associated with a fixed point solution studied by Feigenbaum, Kadanoff, Shenker [Feigenbaum *et al.* (1982)] and by Rand et al. [Ostlund *et al.* (1983)]. Our equation (6) is a two-dimensional generalization of that one. In the present chapter, we will deal with several different fixed points or cycles of this generalized equation. The constant α is specific for each of these solutions (universality classes), and has to be evaluated in a course of numerical solution of the functional equation for each critical situation under study.

As explained in the introductary section, the next step in the RG analysis consists in consideration of dynamics in a vicinity of a fixed-point or cycle solution, i.e., in its stability analysis. For a cycle of period p, $g_1(x,u) \to g_2(x,u) \to ... \to g_p(x,u) \to g_1(x,u)$, we examine a perturbed solution $g_m(x,u) + \epsilon h_m(x,u)$, $\epsilon \ll 1$, and in the first order in ϵ obtain the following equation:

$$\begin{aligned} h_{m+2}(x,u) = \; & \alpha g'_m(\alpha^{-1} g_{m+1}(x/\alpha,\, -uw),\, w^2 u + w)\, h_{m+1}(x/\alpha,\, -uw) \\ & + \alpha^2 h_m(\alpha^{-1} g_{m+1}(x/\alpha,\, -uw),\, w^2 u + w). \end{aligned} \tag{7}$$

Together with the additional condition $h_{m+kp}(x,u) = h_m(x,u)\delta^k$, $m = 1, 2, ...p$, it defines an eigenproblem to extract spectrum of δ values. In particular, for the fixed point case (period $p = 1$) the equation reduces to

$$\begin{aligned} \delta^2 h(x,u) = \; & \alpha\delta g'(\alpha^{-1} g(x/\alpha,\, -uw),\, w^2 u + w) h(x/\alpha,\, -uw) \\ & + \alpha^2 h(\alpha^{-1} g(x/\alpha,\, -uw),\, w^2 u + w). \end{aligned} \tag{8}$$

Usually, the spectrum of eigenvalues requires a careful analysis for the correct interpretation.

First, we account only eigenvalues, which are larger then one in modulus, because the relevant perturbation modes are those, which grow under iterations of the RG transformation.

Second, we must exclude eigenvalues associated with infinitesimal variable changes. For example, a shift $x \to x + \epsilon$, ϵ=const$\ll 1$, produces a variation of the original map, which may be interpreted as a perturbation of a solution of the RG equation. It grows by factor α per step of the RG transformation. A shift $u \to u + \epsilon$ generates a perturbation, which grows by factor β. Obviously, such perturbations are not of interest because they may be removed by a trivial backward variable change.

Third, we must exclude eigenvectors, which correspond to a departure of the solution of the RG equation from the so-called commutative subspace [Ostlund *et al.* (1983)], [Kuznetsov *et al.* (1998)], [Kuznetsov *et al.* (2000)], [Kuznetsov (2002)], [Kuznetsov (2003)]. To explain this point, we remark that, in fact, there exists an alternative way to construct the RG transformation: we could produce the composition of F_m and F_{m+1} steps of iterations *in inverse order*, to obtain $x_{n+F_{m+2}} = f_{m+1}(f_m(x_n,\, u_n), u_n + wF_m)$. It leads to a different, although equivalent form of the whole theory. It is significant, however, that the terms of the functional sequence $f_m(x, u)$ must satisfy a condition of commutativity of the functional pairs, namely, $f_{m+1}(f_m(x_n,\, u_n), u_n + wF_m) = f_{m+1}(f_m(x_n,\, u_n), u_n + wF_m)$, which implies also analogous condition for the renormalized functions g_m. In a course of formal solution of the eigenproblem (8), one gets among others some perturbation modes violating this requirement, and they must be discarded.

Usually, the irrelevant modes can be recognized from observation that their eigenvalues are some combinations of factors α and β.

3 A review of critical points

Let us discuss briefly several critical situations, which may be analyzed in terms of the RG equation (6). As mentioned, functions independent on the second argument represent a particular class of solutions of the functional equation. Of this kind is a solution applicable to the critical point in the circle map discovered by Shenker [Shenker (1982)] and studied in Refs. [Feigenbaum *et al.* (1982)], [Ostlund *et al.* (1983)] by means of the RG analysis. Other examples will correspond to solutions depending on the both two arguments and associated with novel types of critical behavior in quasiperiodically driven maps: a map with pitchfork bifurcation, forced quadratic and circle maps, and forced fractional-linear map.

Classic GM point [Feigenbaum *et al.* (1982)], [Ostlund *et al.* (1983)], [Shenker (1982)]. On the parameter plane of the circle map (Fig.7.1)

$$x_{n+1} = x_n + r + (K/2\pi)\sin 2\pi x_n, \tag{9}$$

the critical line K =1 demarcates a region of regular (periodic or quasiperiodic) dynamics and an area where complex dynamics, including chaos, is possible. Below the critical line, periodic regimes occur inside the Arnold

tongues, and quasiperiodic motions take place between them. They are associated, respectively, with rational or irrational values of the rotation number $\rho(r, K) = \lim_{n\to\infty}(x_n/n)$. There exists a curve of constant golden-mean rotation number: $\rho(r, K) = w = (\sqrt{5} - 1)/2$, which starts at $K = 0$, $r = w$, and meets the critical line $K = 1$ at the GM critical point (GM stands for the 'golden mean'): $K = K_{GM} = 1, r = r_{GM} = 0.60666106\ldots$

Critical point of the blowout birth of SNA [Kuznetsov *et al.* (1995)]. As mentioned, the first example of SNA has been found in a pitchfork bifurcation model with multiplicative quasiperiodic driving, and with a nonlinear function of the hyperbolic tangent [Grebogi *et al.* (1984)]. On reasons of simplification of the subsequent RG analysis, we prefer to introduce a modified model

$$x_{n+1} = \frac{2\lambda x}{\sqrt{1+x^2}} \sin 2\pi n w,\ w = (\sqrt{5} - 1)/2. \tag{10}$$

Qualitatively, the function $x/\sqrt{1+x^2}$ behaves in the same way as $\tanh x$. Therefore, all the arguments for occurrence of SNA remain valid for this map too. As follows, at $\lambda < 1$ attractor is trivial, $x \equiv 0$, and at $\lambda > 1$ it is SNA. The transition called *the blowout birth of SNA* occurs at $\lambda = \lambda_{BO} = 1$, and this is precisely the critical point that may be studied in terms of RG analysis.

Critical points of torus doubling terminal and torus collision terminal [Kuznetsov *et al.* (1998)], [Kuznetsov *et al.* (2000)]. The next model we will consider is a quasiperiodically driven quadratic map [Kaneko (1984)], [Kuznetsov (1984)], [Kuznetsov and Pikovsky (1989)]

$$x_{n+1} = \lambda - x_n^2 + \varepsilon \cos 2\pi n w. \tag{11}$$

Figure 7.2 shows a chart of dynamical regimes for this model on the parameter plane (ε, λ). For $\varepsilon = 0$ Eq.(11) becomes a conventional quadratic map. So, what is observed along the line ε=0 is a usual period-doubling cascade, accumulating to the limit critical point of Feigenbaum (point F) [Feigenbaum (1979)], [Feigenbaum (1983)]. At small but nonzero ε, an increase of λ gives rise to a sequence of torus doubling bifurcations discussed in Chapter 6. A stable fixed point transforms into a stable smooth invariant curve, the torus-attractor T1. Instead of a stable period-2 orbit, we have an attractor consisting of two closed smooth curves, the doubled torus T2. Period-4 orbit, in turn, gives birth to a

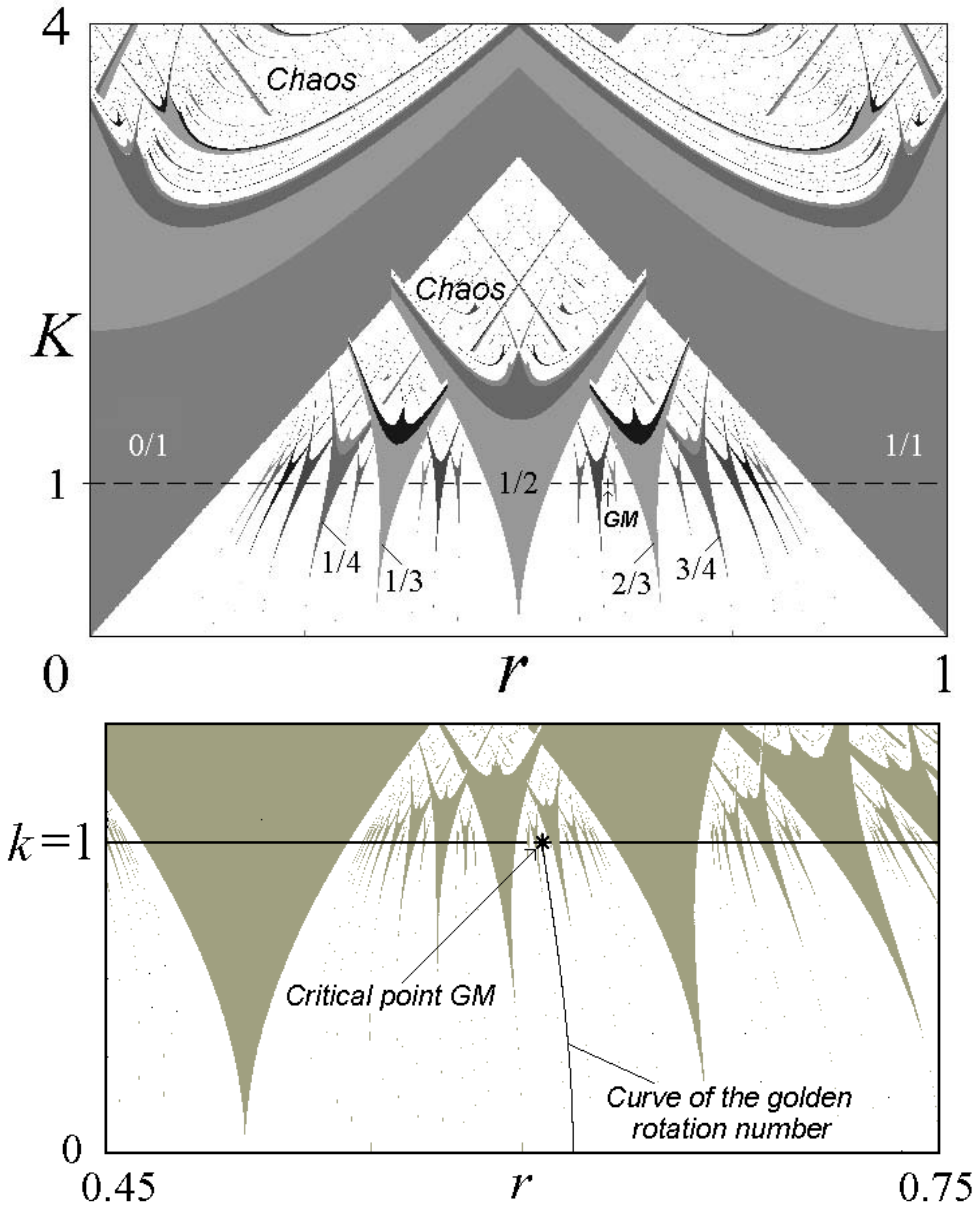

Figure 1: Parameter plane of the circle map (top panel) and explanation of location of the critical point GM (bottom panel). The fractions indicated inside Arnold tongues are respective rotation numbers

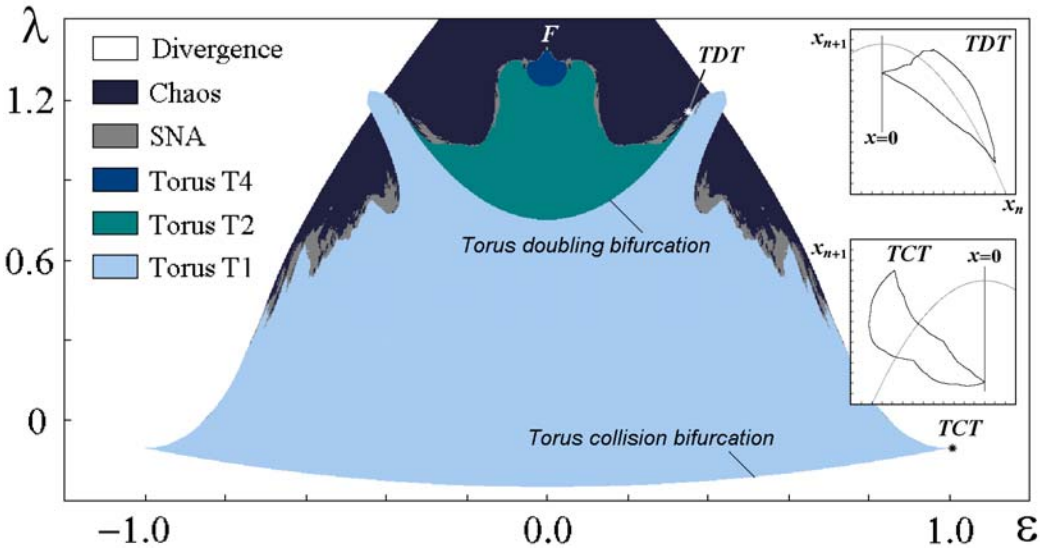

Figure 2: Parameter plane of quasiperiodically driven quadratic map (11). Insets show invariant curves on iteration diagrams as they look at the TDT and TCT critical points. Legend is explained in the left top corner

four-piece invariant curve (torus T4), and so forth. In contrast to usual period-doubling cascade, the sequence of torus doubling is finite: the smaller amplitude of driving, the larger number of the torus doubling bifurcations seen in a course of increase of λ [Kuznetsov *et al.* (1998)], [Kuznetsov *et al.* (2000)], [Kuznetsov (2002)], [Kuznetsov (2003)], [Shenker (1982)], [Grebogi *et al.* (1984)], [Kaneko (1984)]. If we keep λ constant and raise the force amplitude, a smooth torus may transform into SNA. In this transition, the Lyapunov exponent remains negative, but the geometrical structure of the attractor becomes complex, fractal-like. For larger λ and ε, chaotic regimes with positive Lyapunov exponent arise. With further increase of the parameters, the orbits escape to infinity (white domain in Fig.7.2).

On one side, the parameter interval $\lambda \in (-0.25, 0.75)$ corresponding to existence of an attractive fixed point in the unforced quadratic map is bounded by the period-doubling bifurcation, and on another side by the tangent bifurcation associated with a collision of a pair of fixed points (stable and unstable) with their subsequent disappearance. Analogously, for the forced map, the top border of the domain T1 in Fig.7.2 corresponds to the

bifurcation of torus doubling, and the bottom border to the tori collision: an attractor and an unstable set, represented by two invariant curves, approach each other, collide, and disappear.

Let us start at $\varepsilon = 0, \lambda = 0.75$ and move on the parameter plane along the torus-doubling bifurcation curve. While the amplitude of driving is small, the invariant curve born from the fixed point of the unforced system is of small width and placed on one (right) branch of the parabola. As the amplitude increases, the invariant curve grows in width and finally touches the extremum $x = 0$ at some ε. At this moment, the torus doubling bifurcation line is terminated, and we call it the *TDT critical point* ('torus doubling terminal'). It is placed at $\lambda = \lambda_{TDT} = 1.15809685\ldots, \varepsilon = \varepsilon_{TDT} = 0.36024802\ldots$. [Kuznetsov *et al.* (1998)].

Now, let us start at $\varepsilon = 0$, $\lambda = -0.25$ and increase ε to move on the parameter plane along the torus collision bifurcation curve. The situation of collision of smooth invariant curves takes place while the invariant curve is confined on one (left) branch of the parabola. As the amplitude increases, the invariant curve grows in width and touches the extremum $x = 0$ at some ε. This is the critical situation we call the *TCT critical point* ('torus collision terminal'). It is placed at $\lambda = \lambda_{TCT} = -0.09977123\ldots, \varepsilon = \varepsilon_{TCT} = 1.01105609\ldots$ [Kuznetsov *et al.* (2000)].

Critical points of the same kind, TCT and TDT, were found also in quasiperiodically forced circle map

$$x_{n+1} = x_n + r - (K/2\pi)\sin 2\pi x_n + \varepsilon \cos 2\pi n w \,(\mathrm{mod} 1) \tag{12}$$

in supercritical domain $K > 1$, when the mapping near the extrema looks locally just like the parabola map. In some respects, the circle map is a more convenient object for detailed study because no divergence occurs in this map as the variable x is defined modulo 1.

Figure 7.3 shows a chart of dynamical regimes for the driven circle map on a part of the parameter plane (b, ε) including the TCT critical point [Kuznetsov *et al.* (2000)]. The large gray domain in the diagram corresponds to existence of the localized torus attractor. The right border of this domain is the bifurcation curve of collision of a pair of smooth tori, one stable and another unstable. After the event, both of them disappear, and intermittent chaotic regime arises, with a long-time travel through a region of the former existence of the attractor and the unstable invariant set (the 'channel'). Going along the bifurcation curve we see that

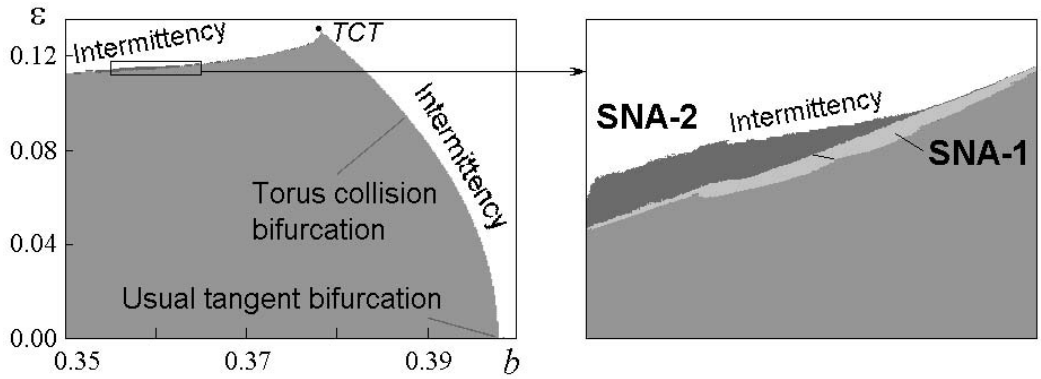

Figure 3: Part of the parameter plane (b, ε) for the driven circle map (12) and an enlarged fragment that shows some subtle details near the intermittent transition

the invariant curve at the situation of collision of the stable and unstable tori, grows in size, and ultimately touches the minimum of the map, there we arrive at the TCT point. As found numerically, it is located at $r = r_{TCT} = 0.377866239\ldots$, $\varepsilon = \varepsilon_{TCT} = 0.132566321\ldots$ A top border of the gray area corresponds to a situation of the intermittent transition from localized to delocalized SNA, with subsequent onset of chaos. The TCT critical point corresponds to the meeting of the bifurcation lines of the two mentioned distinct intermittent transitions.

Critical point of torus fractalization [Kuznetsov (2002)]. As observed, fractalization of torus and transition to SNA in the forced circle map occurs in the critical and subcritical domains at $K \leq 1$ [Kuznetsov (1984)], [Kuznetsov and Pikovsky (1989)]. There, this transition cannot be associated with the TDT or TCT points because of absence of a quadratic exteremum. Nature of the criticality is associated with the *torus fractalization at the intermittency threshold* [Kuznetsov (2002)]. To describe the phenomenon we may use a model

$$x_{n+1} = f(x_n) + b + \varepsilon \cos 2\pi w n, \tag{13}$$

where $f(x)$ is defined as

$$f(x) = \begin{cases} x/(1-x), & x \leq 0.75 \\ 9/2x - 3, & x > 0.75 \end{cases} \tag{14}$$

One branch of the map is selected in a form of the fractional-linear function, $x/(1-x)$, which appears naturally in analysis of dynamics near the tangent bifurcation associated with intermittency (e.g. [Hirsch *et al.* (1982)], [Hu and Rudnick (1982)]). The other branch is attached somewhat arbitrarily, to add the 're-injection mechanism' in the dynamics and to exclude divergence.

Figure 7.4 shows a chart of dynamical regimes for the model (13). The white area designates chaotic regime with positive Lyapunov exponent Λ, and gray regions correspond to negative Λ. In the bottom gray area, attractor is a localized smooth torus. In the left-hand part of the diagram the upper border of this region is a bifurcation curve of transition to a delocalized attractor via intermittency. The bifurcation consists in a collision of smooth stable and unstable tori with their coincidence, and the Lyapunov exponent at the bifurcation is zero. In the right-hand part, the bifurcation curve separates regimes of torus and SNA. Here the bifurcation corresponds to a fractal collision of two invariant curves at some exceptional set of points, which is, nevertheless, dense, and the Lyapunov exponent at the bifurcation is negative. The critical situation takes place at the point separating these two parts of the bifurcation border. We call it *the critical point of torus fractalization* (TF). In the model map (13) it is located at $\varepsilon_{TF} = 2, b_{TF} = -0.59751518\ldots$ [Kuznetsov (2002)].

4 RG analysis of the classic GM critical point

Critical behavior in the circle map associated with break-up of the golden-mean quasiperiodicity (GM critical point) was studied in terms of RG analysis by Feigenbaum et al. and Ostlund et al. [Feigenbaum *et al.* (1982)], [Ostlund *et al.* (1983)]. In a frame of our general scheme, we can consider a set of two uncoupled maps

$$x_{n+1} = f(x_n),\ u_{n+1} = u_n + w \ \ (\mathrm{mod}1), \tag{15}$$

with $f(x) = x + r - (K/2\pi)\sin 2\pi x$. The function f is independent of the argument u, so, the GM criticality will correspond to a degenerate fixed point of our functional equation (6): $g_k(x,u) \equiv G(x)$. In this case, Eq.(6) reads

$$G(x) = \alpha^2 G(\alpha^{-1} G(x/\alpha)), \tag{16}$$

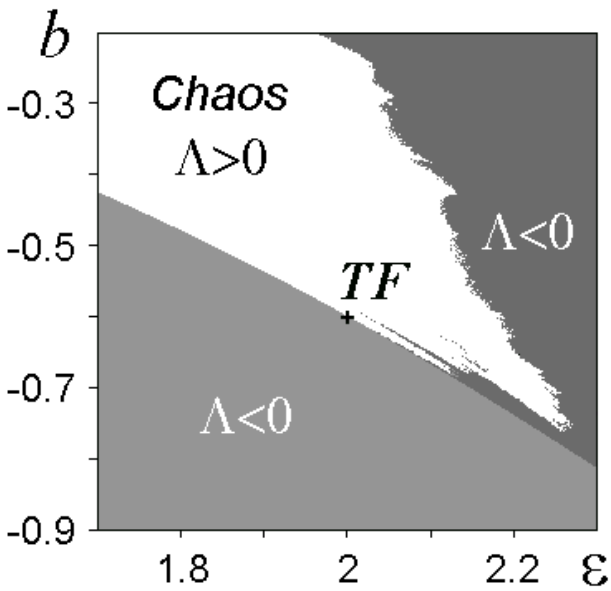

Figure 4: Chart of dynamical regimes for the model (13). The bottom gray area corresponds to a localized attractor represented by smooth torus. The upper border is the bifurcation curve of the intermittent transition. In the left part the bifurcation consists in collision of smooth stable and unstable tori with their coincidence, in the right part – to fractal collision at some exceptional set of points. White area designates chaos, and dark gray presumably corresponds to SNA. Sign of the Lyapunov exponent Λ is indicated in all three domains

and it is known as the Feigenbaum–Kadanoff–Shenker equation. Numerically, the function was found in a form of high-precision expansion in powers of x^3 (e.g. [Feigenbaum *et al.* (1982)], [Ostlund *et al.* (1983)], [Ivankov and Kuznetsov (2001)]. The scaling constant is

$$\alpha = -1.288574553954\ldots \tag{17}$$

Accounting representation of the circle map in the form (15), it is natural to depict the critical attractor in coordinates (u, x). As seen from Fig.7.5, it looks like a fractal curve. Locally, the basic scaling property of this curve may be deduced from the RG analysis. Indeed, the evolution operators for time intervals increasing as Fibonacci numbers are asymptotically identical, up to the scale change. For each next Fibonacci number the variables x and u are rescaled by α and $\beta = -w^{-1}$. As follows, the attractor in coordinates (u, x) must possess self-similarity: increasing resolution in the plot by the factors α and β along the vertical and the horizontal axes, respectively, one can observe similar structures (see the bottom panels of Fig.7.5).

For perturbations of the GM fixed-point, Eq. (8) accepts the form

$$\delta^2 h(x) = \alpha\delta G'(\alpha^{-1}G(x/\alpha))h(x/\alpha) + \alpha^2 h(\alpha^{-1}G(x/\alpha)). \tag{18}$$

As found (e.g. Refs. [Feigenbaum *et al.* (1982)], [Ostlund *et al.* (1983)], [Ivankov and Kuznetsov (2001)]), there are two relevant eigenvalues,

$$\delta_1 = -2.8336106559\ldots,\ \delta_2 = \alpha^2 = 1.660424381\ldots. \tag{19}$$

These constants are responsible for the scaling properties of the parameter space structure near the GM critical point.

In general, to demonstrate two-dimensional scaling, we have to define a special, perhaps curvilinear, local coordinate system near the critical point (*scaling coordinates*). The main requirement is that a displacement along each of two coordinate axes has to give rise to a perturbation of the RG fixed point associated with one of the relevant eigenvalues (19).

In the case of GM critical point it is naturally to conclude that one coordinate line has to go along the critical line $k = 1$, and another one along the curve of constant golden-mean rotation number. Numerically found expressions for parameters of the original map via new coordinates (c_1, c_2) are [Ivankov and Kuznetsov (2001)]

$$r = r_c + c_1 - 0.01749c_2 - 0.00148c_2^2,\ k = k_c + c_2. \tag{20}$$

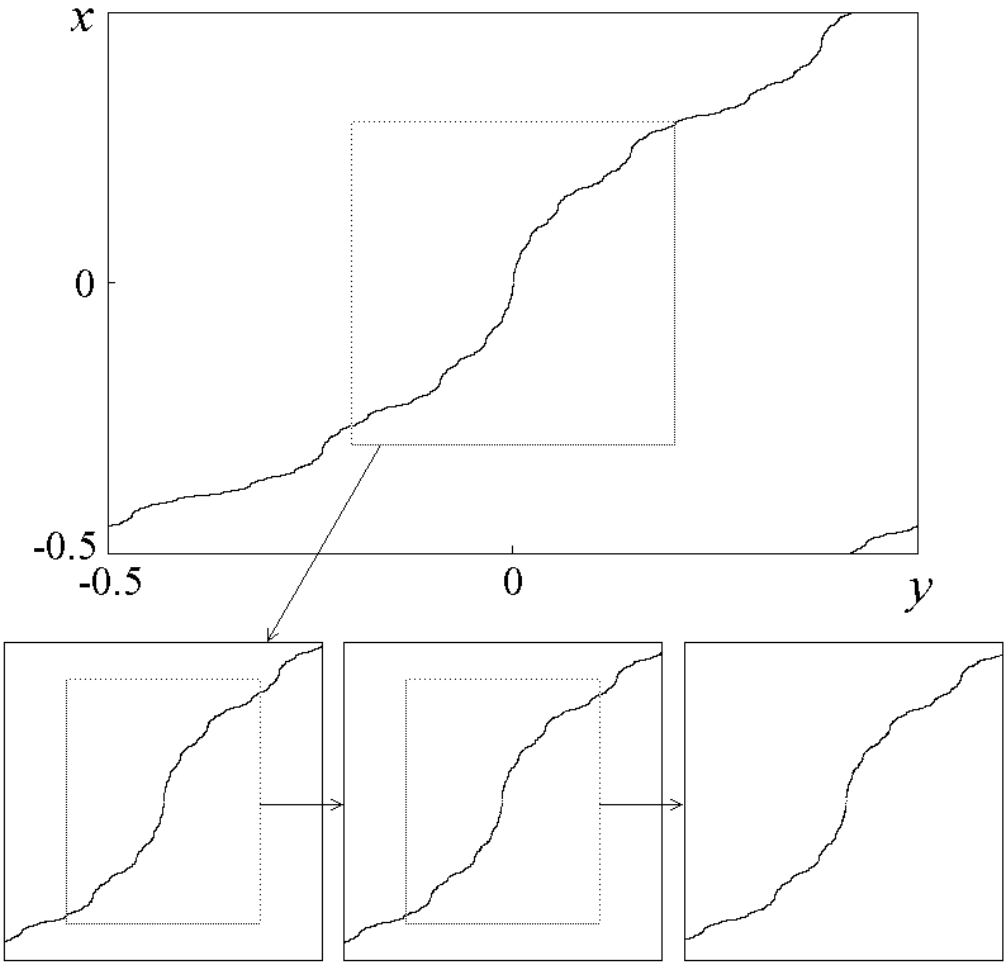

Figure 5: Attractor of the map (15) at the GM critical point (top panel) and illustration of the basic local scaling property: the structure reproduces itself under magnification with factors $\alpha = -1.28857$: and $\beta = -1.61803$: along the vertical and the horizontal axes, respectively

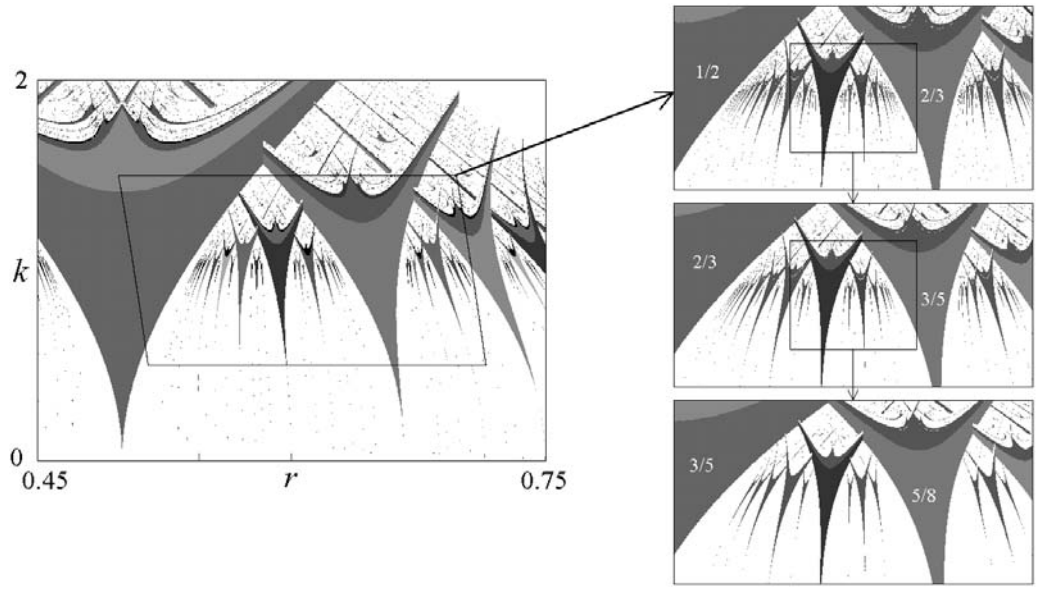

Figure 6: General picture of the parameter plane for the sine circle map and a sequence of fragments for several steps of magnification of a vicinity of the GM critical point in the scaling coordinates, with factors δ_1 and δ_2 along horizontal and vertical axes, respectively

In these equations we retain terms up to the second order because of the relation between δ_1 and δ_2: $\delta_2 < \delta_1$ and $\delta_2 < \delta_1^2$, but $\delta_2 > \delta_1^3$ (see Refs. [Kuznetsov *et al.* (1997)], [Ivankov and Kuznetsov (2001)] for explanation of the rules for selection of the scaling coordinates). Figure 7.6 shows a chart of dynamical regimes with Arnold tongues and a sequence of fragments for several steps of magnification in the scaling coordinates. Observe excellent reproduction of the two-dimensional arrangement of the tongues at subsequent levels of resolution.

5 RG analysis of the blowout birth of SNA

In the pitchfork bifurcation model with multiplicative quasiperiodic driving

$$x_{n+1} = \frac{2\lambda x_n}{\sqrt{1+x_n^2}} \sin 2\pi u_n,\ u_{n+1} = u_n + w\,(\mathrm{mod}1),\ \ w = (\sqrt{5}-1)/2, \quad (21)$$

the bifurcation with transition to SNA occurs at $\lambda = 1$. This is a critical point, which may be studied in terms of our general RG scheme.

A reason for our preference of the nonlinear function used in (21) is that a composition of such functions generates again a function of the same class. Namely, if $f_{1,2}(x) = P_{1,2}x/\sqrt{1+S_{1,2}x^2}$, then $f_1(f_2(x)) = f_3(x) = P_3x/\sqrt{1+S_3x^2}$, where $P_3 = P_1P_2$, $S_3 = S_2 + S_1P_2^2$. This is an important point in a frame of the RG analysis, because for arbitrary number of iteration steps the evolution of the x variable will be given by a function of this special class. In particular, it relates to Fibonacci's numbers of steps, which are of main interest as we deal with the golden mean frequency ratio.

Given a Fibonacci number F_m, we assume that $x_{n+F_m} = f_m(x_n, u_n)$, with $f_m(x,u) = P_m(u)x/\sqrt{1+S_m(u)x^2}$. A subsequent performance of F_{m+1} and then F_m iterations results in F_{m+2} steps, and we must have

$$f_{m+2}(x,\, u) = f_m(f_{m+1}(x,\, u), u + F_{m+1}w) = f_m(f_{m+1}(x,\, u), u - (-w)^{m+1}), \tag{22}$$

or, accounting the composition rules for the considered class of functions,

$$P_{m+2}(u) = P_{m+1}(\,u)P_m(u - (-w)^{m+1}), \tag{23}$$

$$S_{m+2}(u) = S_{m+1}(u) + S_m(u - (-w)^{m+1})\left[P_{m+1}(u)\right]^2. \tag{24}$$

Following our standard construction of the RG scheme, let us change scales of the dynamical variables, $x \to x/\alpha^m$, $u \to (-w)^m u$, where α is a rescaling factor to be determined later, and introduce the renormalized functions

$$g_m(x,u) = \alpha^m f_m(x/\alpha^m,\, (-w)^m u). \tag{25}$$

Here

$$g_m(x,u) = Q_m(u)x/\sqrt{1+H_m(u)x^2}, \tag{26}$$

$$Q_m(u) = P_m((-w)^m u), \tag{27}$$

$$H_m(u) = \alpha^{2m} S_m((-w)^m u). \tag{28}$$

As follows from (22), (25), the functional sequence $g_m(x,u)$ will satisfy our general recurrent RG equation (6), and in terms of the coefficients Q_m, H_m it implies

$$Q_{m+2}(u) = Q_{m+1}(-wu)Q_m(w^2u + w), \tag{29}$$

$$H_{m+2}(u) = \alpha H_{m+1}(-wu) + \alpha^2\left[Q_{m+1}(-wu)\right]^2 H_m(w^2u + w). \tag{30}$$

To perform the functional iterations, it is sufficient to have the involved functions defined on the fundamental interval $u \in [-w, 1]$. Indeed, if u relates to this interval, the same is true for the arguments in the right-hand parts of the equations, $(-wu)$ and $(w^2u + w)$.

Note that the first equation is independent of the second one. Hence, we can decompose the analysis onto two stages: first, we reveal nature of the relevant solution for Q_m, and then examine the second equation, which is linear in H_m. As coefficients, it includes squares $Q_m^2(u)$, so it is convenient to deal directly with them. Obviously, they obey an equation of the same form as (29):

$$Q_{m+2}^2(u) = Q_{m+1}^2(-wu)Q_m^2(\, w^2u + w). \tag{31}$$

To formulate the initial conditions we account that $F_1 = 1$ and $F_2 = 1$, set $P_1(u) = P_2(u) = 2\sin 2\pi u$ (that corresponds to the critical point of the model (21)), and define the rescaled functions, which relate both to *one* iteration step:

$$Q_1^2(u) = 2\sin^2(-2\pi wu),\ Q_2^2(u) = 2\sin^2(2\pi w^2u). \tag{32}$$

To explain what happens under iterations of the RG equation, we follow an elegant scheme developed by Mestel, Osbaldestin and Winn [Mestel *et al.* (2000)] (although these authors deal with another solution of Eq.(29) in a different context than we do). The main idea is to consider step-by-step generation of zeros of the functions at subsequent levels of the construction. The functions under consideration are the so-called entire functions, which are determined completely by distribution of their zeros.

As seen from Eq.(31), presence of a "mother" zero $z^{(m)}$ of a function $Q_m^2(u)$ (at the m-th level) implies appearance of "doughter" zeros in functions $Q_{m+1}^2(u)$ and $Q_{m+2}^2(u)$ relating to the $m+1$-th and $m+2$-th levels, respectively:

$$z^{(m)} \to \begin{cases} z^{(m+1)} = -z^{(m)}/w, \\ z^{(m+2)} = (z^{(m)} - w)/w^2. \end{cases} \tag{33}$$

To start, we account zeros from a fundamental interval $[-w, 1]$, two in the function $Q_1^2(u)$ ($z_1^{(1)} = 0$ and $z_2^{(1)} = 1/2w$) and one in the function $Q_2^2(u)$ ($z_1^{(2)} = 0$). Then, from level to level, they are multiplying, precisely like Fibonacci's rabbits. Note that all zeros we deal with are of order 2 (double degenerate). Selecting some finite interval on the real axis, we can observe that at sufficiently high levels, the generated distributions of zeros manifest

repetition after each 3-th step, in other words, the sets of zeros are identical at m and $m+3$.

It means that the sequence of functions $Q_m^2(u)$ corresponds asymptotically to a period-3 cycle of the RG equation (31). The functions constituting this cycle are products of factors $(u - z_i^{(m+3k)})^2$ over infinite set of zeros generated in asymptotics $k \to \infty$, with appropriately chosen normalization. The valid expression is

$$Q_m^2(u) = \frac{1}{w} \lim_{L\to\infty} \lim_{k\to\infty} \prod_{|z|<L} \frac{(z_i^{(m+3k)} - u)^2}{|(z_i^{(m+3k)} + w)(z_i^{(m+3k)} - w)|}. \tag{34}$$

(The correct normalization is ensured by an expression in denominator, which do not depend on u. It follows from the fact that the periodic solution of (31) must satisfy $Q_m^2(w)Q_m^2(-w) = w^{-2}$, which may be derived from some manipulations with Eq.(31) with taking into account that $Q_m(0) = 0$.)

The second equation, for H_m is linear with periodic coefficients, the period equals 3. So, the asymptotic solution is expected to have a form $H_{3(k+1)+m}(u) = \nu^k H_{3k+m}(u)$, where ν is some constant. Recall that the equation includes a rescaling factor α, yet not determined. We require it to be selected to ensure periodicity of the sequence H_m (i.e., to have $\nu = 1$), and under this condition obtain from (30)

$$\begin{aligned} \alpha^{-2}H_1(u) &= \alpha^{-1}H_3(-wu) + Q_3^2(-wu)H_2(w^2u + w), \\ \alpha^{-2}H_2(u) &= \alpha^{-1}H_1(-wu) + Q_1^2(-wu)H_3(w^2u + w), \\ \alpha^{-2}H_3(u) &= \alpha^{-1}H_2(-wu) + Q_2^2(-wu)H_1(w^2u + w). \end{aligned} \tag{35}$$

This set of equations poses an eigenproblem, where α appears as an eigenvalue, and $H_{1,2,3}(u)$ are components of the eigenvector. To solve it numerically, we represent functions $H(u)$ by tables of their values at nodes of a finite grid on a fundamental interval $[-w, 1]$, and use an interpolation scheme between the nodes. This reduces the set of functional equations to a finite set of algebraic equations. Then, the eigenproblem for a finite matrix may be solved by standard methods of linear algebra. The resulting eigenvalue equals

$$\alpha = 1.09804\ldots, \tag{36}$$

and this is the rescaling factor for x variable per one step of the RG transformation.

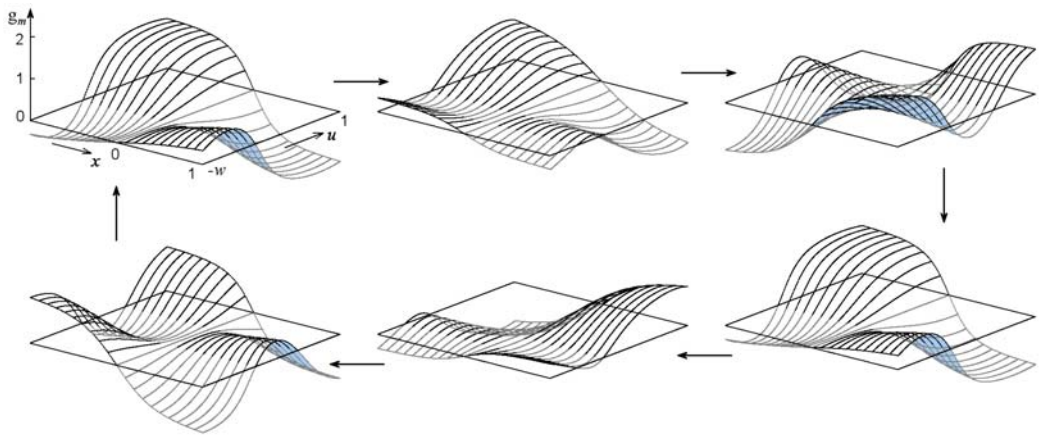

Figure 7: 3D plots of functions $g_m(x,u)$ constituting the period-6 cycle of the RG equation (25).

If we wish to determine functions $g_m(x,u)$, we need $Q_m(u)$ rather than $Q_m^2(u)$. It appears that in respect to index m these functions manifest repetition with period 6, which is twice larger, due to sign changes. As may be shown, they obey relations

$$Q_1(u) = Q_4(u),\, Q_2(u) = -Q_5(u),\, Q_3(u) = -Q_6(u), \tag{37}$$

and then we have

$$g_m(x,u) = Q_m(u)\frac{x}{\sqrt{1+H_m(u)x^2}},\; m = 1,2,...6. \tag{38}$$

These functions constitute a period 6 cycle of the RG equation as illustrated in Fig.7.7. A sense of $g_m(x,u)$ is that it determines a rescaled evolution operator for F_{m+6k} iterations of the original map at the critical point in asymptotics $k \to \infty$. Cyclic repetition of the functions implies presence of scaling regularities, i.e. of similarity of the dynamics on different time scales. However, formulating these scaling properties, we may regard the dynamics similar not after six, but after three steps of the RG transformation: although functions $g_m(x,u)$ and $g_{m+3}(x,u)$ can differ in sign, this is not essential because the model under study is symmetric in respect to a change $x \to -x$.

Three steps of the RG procedure correspond to increase of time scale by factor $\tau_m = F_{m+3}/F_m$, asymptotically $\tau = 1/w^3 = 4.236068$. Now, if we

observe dynamical evolution starting from some x and u, then, we get similar dynamics with time scale multiplied by τ, if start from x/a and u/b, where $a = \alpha^3 = 1.32390$ and $b = 1/(-w)^3 = -4.236068$ are the phase space scaling factors.

The only observable kind of dynamics precisely at the critical point is a transient to final trivial stationary state $x = 0$. From the above statements we conclude that this decay must follow a power law, $|x_n| \propto n^{-\gamma}, \gamma = \log a / \log \tau = 0.19436$.

These notes relate to a vicinity of $u = 0$, at which the scale transfomation was defined in our derivation of the RG equation. At other initial phases, the scalings may be different (this reflects a multifractal nature of the SNA that borns in a coarse of the transition under study). In particular, with one iteration of the original map, a point (x, u) from a vicinity of $u = 0$ is mapped to a neighborhood of $u = w$, with multiplication of x by $\sin 2\pi u \propto u$. Thus, the scaling factor for x near this new point will be a product of factors for x and u at the old point, namely, $a' = ab = \alpha^3/w^3 = 5.60809$. Respectively, decay of x near $u = w$ will follow a distinct power law $|x_n| \propto n^{-\gamma'}, \gamma' = \log a' / \log \tau = \gamma + 1 = 1.19436$.

Figure 7.8 illustrates scaling regularities intrinsic to the critical decay. Absolute values of x generated by the map (21) at $\lambda = 1$, are plotted versus discrete time n in the double logarithmic scale. Observe that the region occupied by the plotted points is bounded from above and from below by straight lines corresponding to the power laws $|x_n| \propto n^{-\gamma}$ and $|x_n| \propto n^{-\gamma'}$. Evidently, γ and γ' are just the largest and the smallest numbers among the critical indices associated with the decay at the threshold of SNA birth.

The second part of the RG analysis consists in consideration of a perturbation for the periodic solution, – a departure from the critical point.

Let us search for solution of the equation (29) as $Q_m(u) + \epsilon \tilde{Q}_m(u)$, $\epsilon \ll 1$. In the first order in ϵ we get

$$\tilde{Q}_{m+2}(u) = \tilde{Q}_{m+1}(-wu) Q_m(w^2 u + w) + Q_{m+1}(-wu) \tilde{Q}_m(w^2 u + w). \quad (39)$$

In terms of our RG formalism, a shift of parameter $\lambda \to 1 + \Delta\lambda$ in the model map (21) corresponds to multiplication of $Q_1(u)$ and $Q_2(u)$ by $1+\Delta\lambda$. As may be checked by direct substitution, a solution with initial conditions $\tilde{Q}_{1,2}(u) = Q_{1,2}(u)\Delta\lambda$ is $\tilde{Q}_m(u) = Q_m(u) F_m \Delta\lambda$. In a course of iterations of the RG equation, the same function (up to a sign) appears again after three steps, but multiplied by factor F_{m+3}/F_m. In asymptotics, this ratio yields a

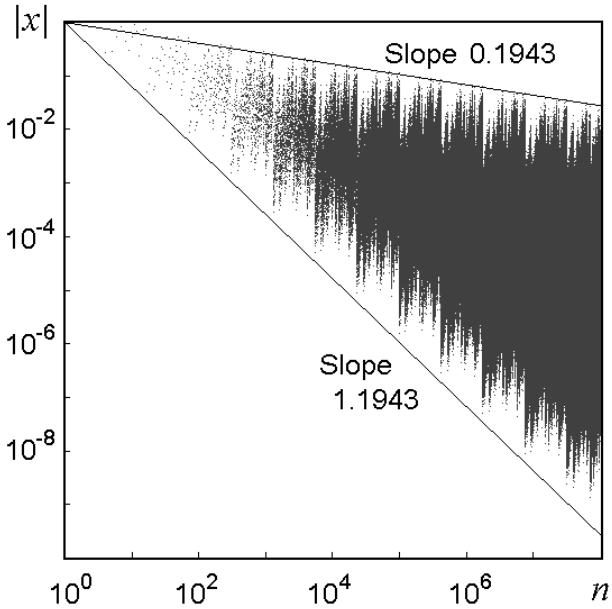

Figure 8: Absolute value of the dynamical variable x versus discrete time at the critical parameter value $\lambda = 1$ plotted in double logarithmic scale. Initial value $x = 1$. Note that observed values of x are bounded from above and from below by straight lines corresponding to power laws $|x| \propto n^{\gamma}$ and $|x| \propto n^{\gamma'}$, respectively

constant for renormalization of the parameter deflection

$$\delta = 1/w^3 = 4.236068. \tag{40}$$

(We may not consider the second equation for $H(u)$, as the present argumentation is sufficient to get δ.)

Now we formulate a scaling ptoperty accounting the parameter shift in respect to sustained dynamical regimes. Let us suppose that at a parameter value $\lambda = 1 + \Delta\lambda$ close to the critical point we observe some dynamical regime, the SNA (see argumentation in Chapter 2). Now, decreasing $\Delta\lambda$ by factor $\delta = 1/w^3$, we come to a situation, when the evolution operator is similar to the original one, but with time scale increased by $\tau = 1/w^3 = 4.236068$, scale in x decreased by $a = \alpha^3 = 1.32390$, and scale in u reduced by $b = 1/(-w)^3 = -4.236068$. Been drawn in the rescaled coordinates, the SNA will look like the original one. (In fact, the scaling property is asymptotical: the closer λ to the critical point, the more accurate is the similarity.)

Figure 7.9 illustrates the stated scaling property of attractors in a vicinity of the critical point. The computed portraits of SNAs are plotted: dynamical variable x versus phase variable u. Each next picture corresponds to smaller distance from the critical point, decreased by factor δ, and is shown with magnification by factors a and b along the vertical and horizontal axes, respectively. Observe remarkable similarity of the pictures with reproduction of all subtle details of the structure of the SNAs.

On a basis of scaling argumentation, one can derive a relation for extension of a size of SNA under increase of the parameter near the transition. For this, we have to use the scaling relations stated for a vicinity of $u = 0$. Apparently, these will be the largest absolute values of x in the attractor at phases near $u = 0$, as they have been growing on previous iterations without vanishing of the multiplicative driving term $\sin 2\pi u$ (the strong decay will occur just at the next step). So, under reduction of the distance from the critical point by $\delta = 4.236068$, a size of attractor will decrease by factor $a = 1.32390$. That implies the power law relation $|x| \propto \Delta\lambda^\gamma$, $\gamma = \log a / \log \delta \approx 0.1943$ (the same index as obtaned for the critical decay near zero phase).

In Fig.7.10a we present a 3D bifurcation diagram illustrating the birth of SNA, the absolute value of x versus phase u and parameter λ. One can clearly see that the grows of size of the attractor has essentially different rates in dependence on phase, but it is the most rapid at $u = 0$. Fig.7.10b demonstrate verification of the suggested relation: the maximal absolute

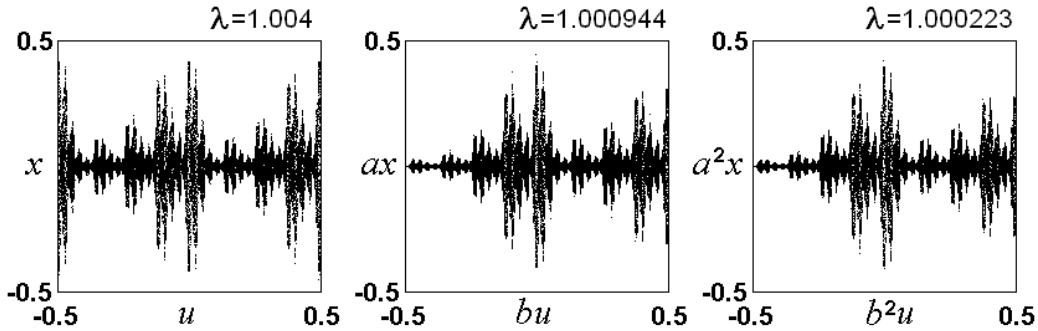

Figure 9: Illustration of scaling of attractors in a vicinity of the critical point. Portraits of SNAs are shown at three parameter values; each next plot corresponds to decrease of deflection from the critical point by factor $\delta = 4.2361$ and scale change along the vertical and horizontal axes with factors $a = 1.3239$ and $b = -4.2361$, respectively. The negative factor b corresponds to inversion of the picture along the horizontal axis

value of x over the whole attractor is plotted versus parameter deflection from the critical point in double logarithmic scale. Observe that the numerical data follow well the predicted straight line with slope γ.

To finish this section, we remark that the tangent hyperbolic map suggested in the first original paper on SNA of Grebogi et al. [Grebogi *et al.* (1984)]

$$x_{n+1} = 2\lambda \tanh x_n \sin 2\pi\theta_n,\ \theta_{n+1} = \theta_n + w\,(\mathrm{mod}1), \tag{41}$$

demonstrates the same scaling regularities at the point of the birth of SNA and for sure relates to the same universality class.

However, more rich behavior is observed in a generalized model suggested by Glendinning [Glendinning (2002)]

$$x_{n+1} = 2\lambda(\cos 2\pi\theta_n + p)\tanh x_n,\ \theta_{n+1} = \theta_n + w\,(\mathrm{mod}1), \tag{42}$$

The parameter plane (λ, p) of this map (Fig.7.11) contains three areas: one of the existence of the trivial attractor $x \equiv 0$, the second of SNA, and the third of a smooth torus-attractor. The transition from trivial attractor to SNA occurs at the bifurcation border $\lambda = 1$ in the interval of p from 0 to 1. The scaling regularities examined above in this section take place at $p = 0$. On the rest part of the bifurcation border $\lambda = 1$ they modify because of the

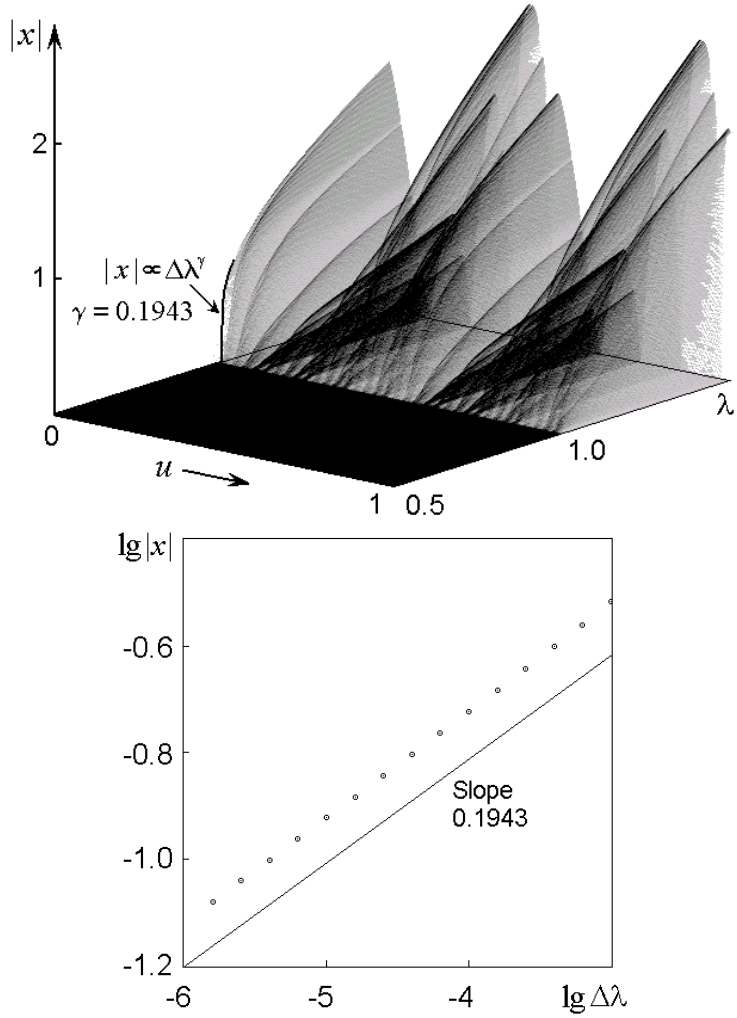

Figure 10: A diagram of the absolute value of x versus phase u and parameter λ illustrating the birfh of SNA in the model map (21) (a) and verification of the relation for the attractor size at $u = 0$ in double logarithmic scale (b)

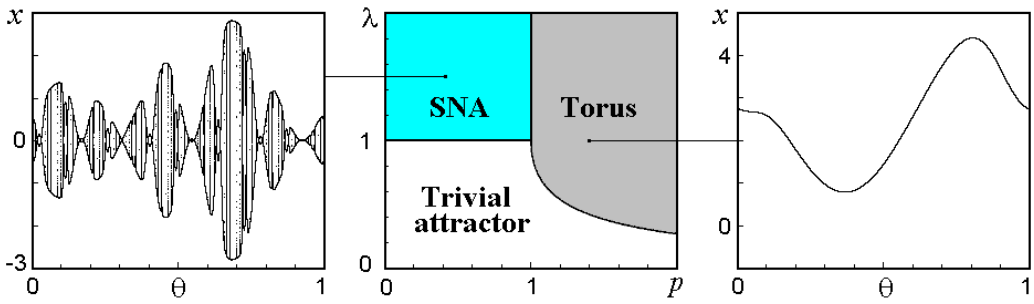

Figure 11: Parameter plane of the modified hyperbolic tangent map with quasiperiodic driving (42) with marked areas of trivial attractor $x \equiv 0$, SNA, and torus. Examples of the phase portraits of SNA and torus are shown in two side panels

distinct location of zeros of the functions $Q(u)$ (see (32)). At the edge of the bifurcation border $p = 1$, a critical point of higher codimension obviously presents. This example shows that further researches are desirable to reveal completely all possibilities that can occur in the case of the blowout transition to SNA in the most general circumstances.

6 RG analysis of the TDT critical point

In this section, we consider the torus-doubling terminal point (TDT) [Kuznetsov *et al.* (1998)], which occurs in the forced quadratic map

$$x_{n+1} = \lambda - x_n^2 + \varepsilon \cos 2\pi u_n,\ u_{n+1} = u_n + w \ (\mathrm{mod} 1). \tag{43}$$

In contrast to the previous case of the blowout transition, a nontrivial numerical problem is to locate the critical point in the parameter plane accurately. To carry out this necessary preliminary step to the RG analysis, let us recall a definition of the TDT point.

In the unforced map, at the first doubling bifurcation we have a fixed point at the stability threshold. For small amplitudes of driving, it turns into a smooth invariant curve placed entirely in the region $x > 0$ (Fig. 7.12). Let us suppose that we increase the amplitude and go along the bifurcation curve in the parameter plane, where the birth of the doubled torus T2 takes place from the original torus T1. In a course of this motion, the invariant curve becomes wider and wider, and the minimum value of x on it approaches and

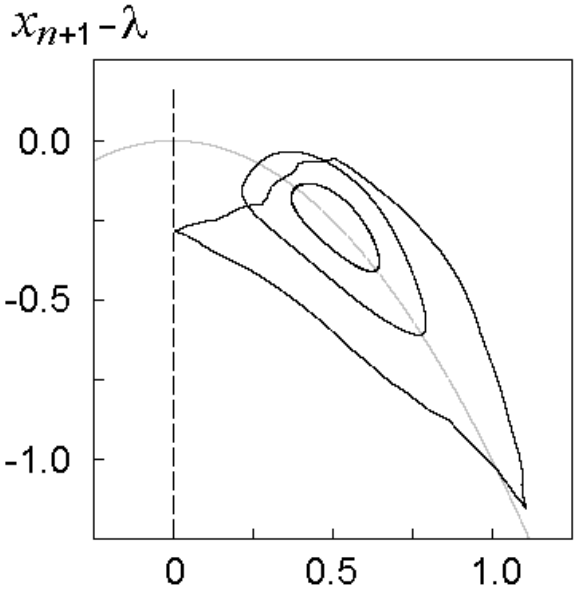

Figure 12: Tori at the threshold of the doubling bifurcation: smooth tori for $\varepsilon = 0.1$, $\lambda = 0.778791$ and $\varepsilon = 0.2$, $\lambda = 0.824501$, and the critical torus for ε_c, λ_c. For visual clarity, the vertical coordinate is shifted by λ, so the graph of the quadratic map has the same form for all parameter values. The critical torus touches the line $x = 0$

finally reaches zero. This event just corresponds to the TDT critical point. As we are at the bifurcation curve, a typical orbit on the torus is just at the instability threshold. On the other hand, the touch with zero implies appearance of a superstable orbit on the torus, the one, which contains the parabola maximum $x = 0$.

Let us consider the situation in terms of rational approximations of the frequency parameter by ratios of Fibonacci numbers. For a rational frequency $w_m = F_{m-1}/F_m$, we get a cycle of period F_m instead of the T1 torus. Increasing the control parameter λ we expect to see a bifurcation of this cycle at some parameter value that approximates the torus-doubling bifurcation. In fact, the bifurcation point for the rational frequency w_m will depend on the initial phase u_0. Asymptotically, for $m \to \infty$, we can speak on the torus-doubling bifurcation only if the limit does not depend on u_0. Certainly, this is the case at small amplitudes ε. We may gradually increase ε and trace the

torus-doubling curve as long as possible.

Let us state formal conditions of the situation in terms of rational approximations. At a fixed rational frequency $w_m = F_{m-1}/F_m$, we impose the following two requirements.

(i) For some initial phase $u_0 = u^0$ there exists a period-F_m cycle starting from $x = 0$, and the derivative dx/du_0 vanishes. This cycle will be superstable, with zero Floquet multiplier. (The condition of zero derivative means a touch of the line $x = 0$ by the approximate torus: nearby orbits do not intersect this line.)

(ii) Minimum of the Floquet multiplier reached at some other initial phase u^1 equals (-1), i.e., for this phase the cycle of period-F_m is at the threshold of the period-doubling bifurcation. (Of course, this may be true only for the approximants with odd Fibonacci's denominators; therefore, we consider at this moment only them.) In the limit of the irrational frequency parameter, this corresponds to a condition of the torus-doupling bifurcation.

In Table 7.1 we summarize the computational data, which show evident convergence. The estimate of the limit yields location of the TDT point. Additionally, one can observe from the table a convergence of the phase sequence u^0 to a definite limit, which is also significant. (Note that a limit for u^1 values is the same.) Our best result for these limits, improved with a technique based on further results of the RG analysis, is

$$\lambda_c = 1.158096856726,\ \varepsilon_c = 0.360248020507,\ u_c = 0.3952188264. \qquad (44)$$

At a point from the Table 7.1 with a rational frequency w_m, we have simultaneously a superstable cycle at one phase, and a cycle at the period-doubling bifurcation threshold at another. Obviously, by an infinitesimal parameter shift from this point we can reach a situation that the cycle remains stable at one phase and becomes unstable at some other. This means inevitable occurrence of bifurcations in dependence on the phase of the external force, which persist at all levels of the rational approximation. According to the criteria formulated in Chapter 3 (see also [Pikovsky and Feudel (1995)]), we conclude that a small parameter variation from the TDT point can give rise to an SNA. Additionally, numerical computations show that chaotic states appear in a neighborhood of the TDT point. Finally, as clear from our way

Table 1: Numerical data for the torus doubling terminal point in rational approximations for the driven quadratic map map (43)

w_m	λ	ε	$2\pi u^0$
2/3	0.89313590	0.39045526	2.38814031
3/5	1.07633288	0.30511453	2.27096915
8/13	1.14077398	0.35637173	2.47438570
13/21	1.13453832	0.35326266	2.51704366
34/55	1.15587157	0.36021207	2.48341089
55/89	1.15364997	0.35864970	2.47129447
144/233	1.15790681	0.36022344	2.48295110
233/377	1.15720706	0.35995120	2.48531755
610/987	1.15807555	0.36024655	2.48328049
987/1597	1.15796494	0.36019031	2.48259605
2584/4181	1.15809462	0.36024806	2.48321966
4181/6765	1.15806354	0.36023723	2.48335560
10946/17711	1.15809658	0.36024835	2.48323605

of reasoning, quasiperiodic regimes of type T1 and T2 also take place in its vicinity. Therefore, significance of TDT point is that a complete set of relevant dynamical regimes of the system occur arbitrarily close to it. It is natural to think that details and regularities of dynamical behavior in this special local region of the parameter space are of principal importance for understanding general properties of dynamics in the model under study, and, moreover, in the entire universality class associated with this type of critical behavior.

As a next step, let us consider a procedure aimed to reveal the nature of the solution of the RG equation responsible for the behavior at the TDT critical point. First of all, we introduce a coordinate system on the phase plane (x, u) appropriate for constructing the RG transformation. It is natural to place the origin at $x = 0$, $u = u_c$. Indeed, the value $x = 0$ is an extremum of the forced one-dimensional map, obviously, a point of special significance, and u_c is the limit point of the phases for a sequence of cycles, superstable or bifurcating, on the approximated tori. We do not change the directions of the coordinate axes, so, the new coordinates are simply $X = x$ and $Y = u - u_c$. Now, we can compute terms of the functional sequence $g_m(X, Y)$ by virtue

of straightforward iterations of the original maps (43) at the critical point. Given a sufficiently large Fibonacci number F_m (say, 233), we first set the initial condition $x_0 = 0$, $u_0 = u_c$ and iterate the mapping F_m times. The resulting $x_{Fm} = x^0_{Fm}$ determines a normalization factor used later. Now, to obtain the value of $g_m(X, Y)$ for some particular X and Y, we iterate the map (43) again, but with initial conditions $x_0 = x^0_{Fm}X$, $u_0 = (-w)^m Y$. After F_m iterations we get $g_m(X, Y) = x_{Fm}/x^0_{Fm}$. Such computations show that for high-order Fibonacci numbers the functions $g_m(X, Y)$ form a sequence of period 3: $g_m(X, Y) \approx g_{m+3}(X, Y)$. Therefore, we conclude that this is the period-3 solution of the RG equation, which responds for the critical behavior at the TDT point. Moreover, the computations yield an estimate for the factor of renormalization for x variable, $\alpha^3 \cong x_{Fm}/x_{Fm+3} \cong 3.96$.

The next step is to get an accurate numerical solution of the functional equation (6). For this, we approximate the functions of two variables constituting the period-3 cycle $g_1(X, Y) \to g_2(X, Y) \to g_3(X, Y) \to g_1(X, Y)$ by finite polynomial expansions with unknown coefficients, and one more unknown is factor α. The expansions contain odd and even powers of Y and even powers of X. One of the three functions is assumed to be normalized to unity, say $g_1(0, 0) = 1$. Then, the procedure of RG transformation is organized as a computer program operating with the expansion coefficients. It corresponds to an implicitly defined finite set of nonlinear algebraic equations. This set is solved by means of a multi-dimensional quasi-Newton method. The crucial point is to have a good initial guess for the unknowns; we take them from the numerical estimates for the functions g_m and the constant α, described in the previous paragraph.

The final result is representation of a functional pair $\{g_1(X, Y),\ g_2(X, Y)\}$ in a form of polynomial expansions over X and Y. (The third function can be computed easily from the functional composition rule following from the basic equation (6).) The concrete expressions are too tedious to present them here (see the table of coefficients published in Ref. [Bezruchko *et al.* (1997)] and at the web page http://www.sgtnd.narod.ru/science/alphabet/eng/goldmean/tdt.htm). Figure 7.13 shows a series of 3D plots illustrating this solution. The most accurate estimate for the rescaling factor obtained from the computations is

$$\alpha = 1.58259341\ldots. \tag{45}$$

A function $g_m(X, Y)$ determines a rescaled evolution operators for F_{m+3k} iterations of the driven quadratic map at the TDT critical point (in fact,

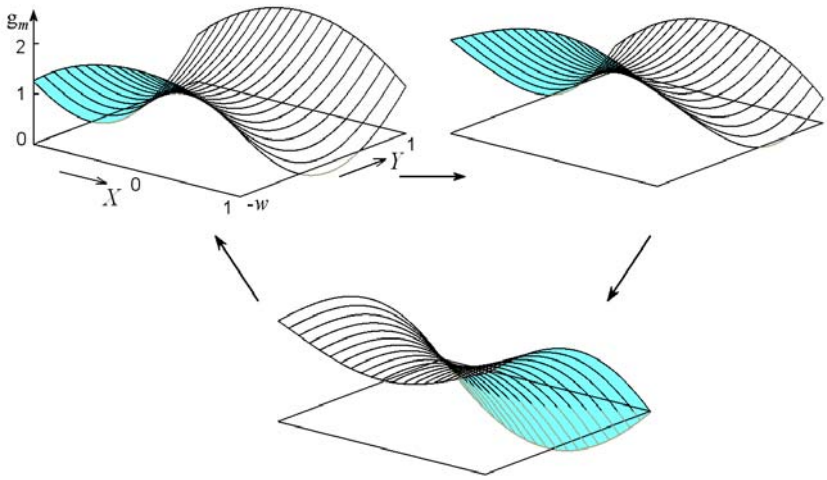

Figure 13: 3D plots of functions $g_m(X, Y)$ constituting the period-3 cycle of the RG equation associated with the TDT critical point

in the asymptotics $k \to \infty$). Cyclic repetition of these functions implies presence of scaling regularities, i.e. similarity of the dynamics on different time scales. Three steps of the RG procedure correspond to increase of the time scale by a factor $\tau_m = F_{m+3}/F_m$, asymtotically $\tau = 1/w^3 = 4.236068$, and rescaling of x and u variables by factors $a = \alpha^3 = 3.96376647$ and $b = 1/(-w)^3 = -4.236068$. It means that iterations of the forced quadratic map at the critical values of λ and ε starting from some x and u, and those starting from x/a and $u_c + (u - u_c)/b$ demonstrate similar dynamics. In the second case the time scale is greater by τ, and the phase space scales for x and u are less, by factors a and b, respectively.

While we move on the parameter plane from small driving amplitude to the TDT point, following the torus-doubling bifurcation border, the invariant curve remains smooth (Fig.7.12). As we reach the TDT point, the invariant curve becomes fractal-like. We call it the *critical attractor* and show it in Fig.7.14 in coordinates (u, x).

As follows from the RG analysis, the critical attractor must demonstrate self-similarity, and we can explicitly formulate this property in a vicinity of the point $x = 0$, $u = u_c$ ('*the scaling center*'). If we rescale $X = x$ and $Y = u - u_c$, respectively, by a and b, the curve representing the attractor must be locally invariant under this transformation. As seen from Fig.7.14, this is indeed the case: picture inside a selected box reproduces itself under

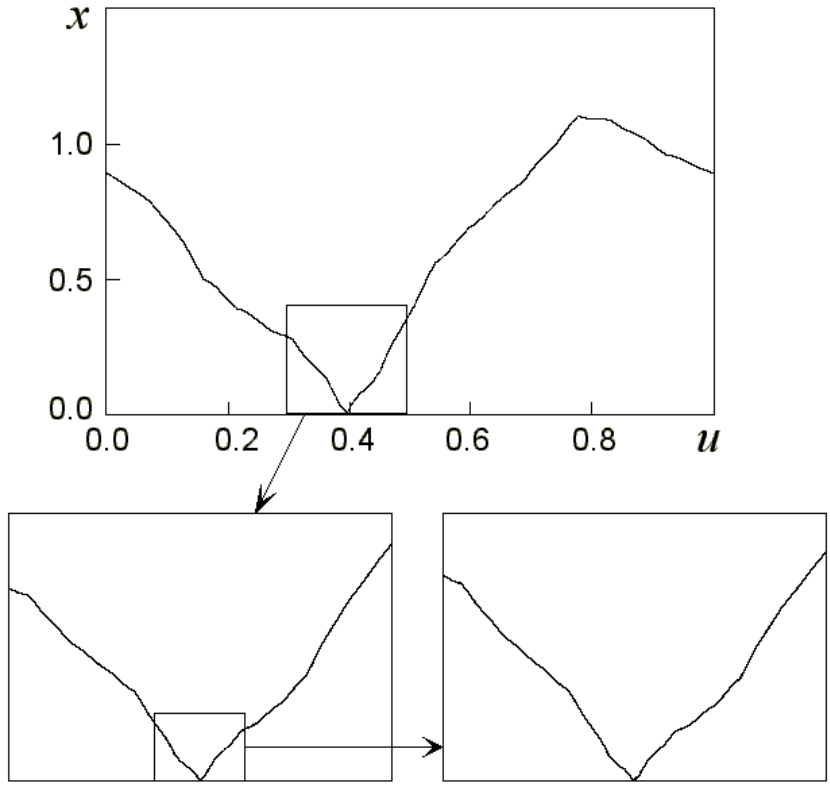

Figure 14: Attractor of the forced quadratic map at the TDT critical point (the top panel) and illustration of the basic local scaling property: the structure reproduces itself under magnification with factors $a = \alpha^3 = 3.96376$ and $b = \beta^3 = -4.2360$ along the vertical and the horizontal axes, respectively. The negative scaling factor b implies reflection along the horizontal axis

subsequent magnifications by the factors a and b. To possess the stated scaling property, the invariant curve must behave locally as $x \propto |\Delta u|^{\kappa}$ with $\kappa = \log\alpha/\log|\beta| \cong 0.954$. The exponent κ is close to 1, so visually the curve looks like broken at the point of singularity. It is important to remark that due to ergodicity of the quasiperiodic motion, the singularity at the origin implies presence of singularities of the same type at all points, to which it is mapped under subsequent iterations of the map. This is a dense set of points on the invariant curve. As κ is less than 1, the invariant curve in nowhere differentiable. Thus, the conclusion on fractal nature of the critical attractor follows directly from the results of the RG analysis.

Stability analysis in terms of the linearized RG equation for the period-3 cycle solution responsible for the TDT criticality gives rise to the following eigenvalue problem:

$$\begin{aligned}
h_3(X,Y) = \quad & \alpha g_1'(\alpha^{-1}g_2(X/\alpha,\, -Yw),\, w^2Y+w)h_2(X/\alpha,\, -Yw) \\
& +\alpha^2 h_1(\alpha^{-1}g_2(X/\alpha,\, -Yw),\, w^2Y+w), \\
\delta h_2(X,Y) = \quad & \delta\alpha g_3'(\alpha^{-1}g_1(X/\alpha,\, -Yw),\, w^2Y+w)h_1(X/\alpha,\, -Yw) \\
& +\alpha^2 h_3(\alpha^{-1}g_1(x/\alpha,\, -yw),\; w^2Y+w), \\
\delta h_1(X,Y) = \quad & \alpha g_2'(\alpha^{-1}g_3(X/\alpha,\, -Yw),\, w^2Y+w)h_3(X/\alpha,\, -Yw) \\
& +\alpha^2 h_2(\alpha^{-1}g_3(X/\alpha,\, -Yw),\, w^2Y+w),
\end{aligned} \tag{46}$$

where δ is the eigenvalue, and $h_{1,2,3}(X,Y)$ are functions constituting the eigenvector. Numerical solution of this problem is based on approximation of $h_{1,2,3}(X,Y)$ by finite polynomial expansions, with substitution of $g_{1,2,3}(X,Y)$ and α, which are already known. On this way, we reduce the functional eigenproblem to that for a finite matrix, which allows a solution with standard methods of linear algebra. After excluding irrelevant eigenvalues (which are either less than 1 in moduls, or associated with infinitesimal variable changes or with departures from the commutative subspace) we have the following two eigenvalues in the rest:

$$\delta_1 = 10.5029\ldots \text{ and } \delta_2 = 5.1881\ldots \tag{47}$$

They have a sense of scaling factors responsible for properties of self-similarity in arrangement of the parameter plane near the TDT critical point.

To observe the scaling regularities in a vicinity of the critical point we need to define an appropriate local coordinate system ('scaling coordinates'). As origin, we naturally take the point TDT itself. Then, the coordinate axes should be directed in such way that a shift along the first one generates the

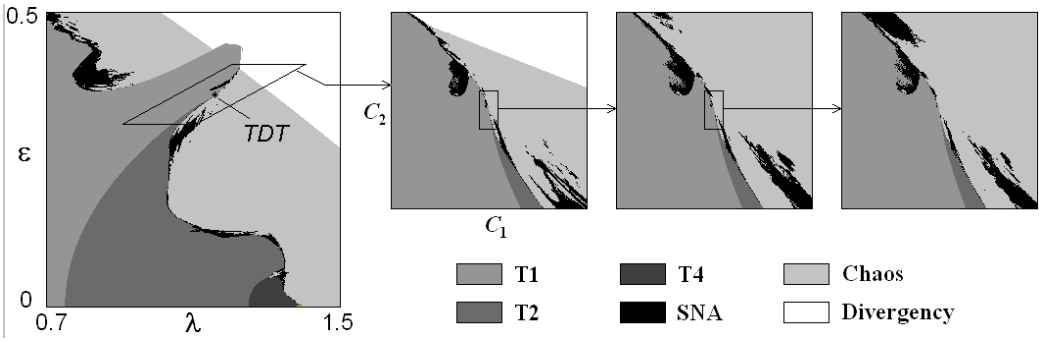

Figure 15: Chart of dynamical regimes on the parameter plane of the quasiperiodically driven quadratic map and a sequence of fragments for several steps of magnification of a vicinity of the TDT critical point in the scaling coordinates, with factors δ_1 and δ_2 along the horizontal and vertical axes, respectively. Gray area corresponds to localized attractor with negative Lyapunov exponent, and white to chaos

mode of perturbation of evolution operators associated with δ_1, and the mode with δ_2 is produced with a shift along the second axis. In such coordinate system the configuration of regions in the parameter plane near the TDT point will be self-similar and will reproduce itself locally under scale change along the coordinate axes by δ_1 and δ_2, respectively.

In fact, an axis, corresponding to the larger eigenvalue δ_1 may be defined almost arbitrarily, say, as a direction along the λ axis, but the second one must be selected very carefully to exclude a contribution of the first eigenmode into the solution on this axis. As found numerically, for our model (43), appropriate new coordinates (c_1, c_2) and parameters (λ, ε) are linked as follows:

$$\lambda = \lambda_c + c_1 + c_2,\ \varepsilon = \varepsilon_c + 0.3347 c_2. \tag{48}$$

(For our purposes of demonstrating scaling in the case of TDT point it is sufficient to use a linear parameter change because of the relation between the relevant eigenvalues: $\delta_2 < \delta_1$ and $\delta_2 > \delta_1^m$ for $m = 2, 3, \ldots$).

Figure 7.15 shows a chart of dynamical regimes for the driven quadratic map (43) near the TDT point in scaling coordinates for several steps of subsequent magnification.

Figure 7.16 illustrates the scaling property with Lyapunov charts, where values of the nontrivial Lyapunov exponent are shown by gray tones. The

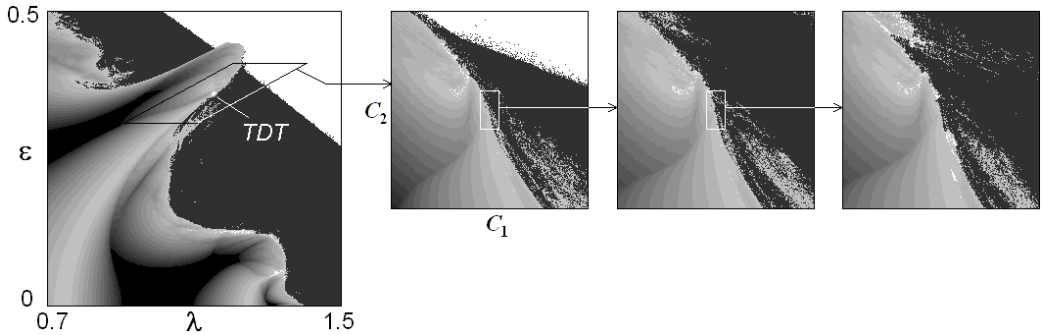

Figure 16: Scaling in the vicinity of the critical point illustrated by the Lyapunov charts. The Lyapunov exponent is coded in gray scale. Left panel: a region around the TDT point in natural coordinates. The interior of the parallelogram is shown separately in the scaling coordinates for several steps of magnification with factors δ_1 and δ_2 along the horizontal and vertical axes, respectively. The gray coding for the Lyapunov exponent is scaled with the factor τ

Lyapunov exponent is inversely proportional to characteristic time scale. Therefore, to outline the similarity of the pictures, the coding rule is redefined at each next level of magnification in such way that it corresponds to rescaling of the Lyapunov exponent by factor τ.

Observe good correspondence of the pictures at higher levels of magnification under scale change by factors δ_1 and δ_2 along the axes of scaling coordinates. It means that configuration of the regions in the parameter plane indeed obeys the expected property of self-similarity. In particular, it follows that all the regimes: T1, T2, SNA, chaos, occur arbitrarily close to the critical point.

As expected, the regularities intrinsic to dynamics at the TDT critical point and in its vicinity are universal; in particular, this relates to the estimated numerical values of the scaling constants. Therefore, this type of critical behavior has to occur in many nonlinear dissipative system manifesting the period-doubling bifurcation cascade, in presence of additional periodic force of the incommensurate frequency (the golden-mean frequency ratio). Heuristically, the hypothesis of universality follows from the RG argumentations, in the same spirit as the Feigenbaum universality for classic period doubling [Feigenbaum (1979)], [Feigenbaum (1983)].

An essential attribute of the TDT universality class is certain definite

parameter plane topography in a vicinity of the critical point. Depicted in scaling coordinates it will be universal, and on this reason it deserves a special attention. The consideration reveals some links with bifurcation scenarios in quasiperiodically forced systems mentioned in Chapter 5.

In the left top panel of Fig.7.17 we reproduce in scaling coordinates a sketch of the parameter plane arrangement near the TDT point. On the roads marked (a), (b), and (c) one can observe the bifurcation scenarios involving SNA; see other panels of the figure. In the bifurcation diagrams, horizontal axis corresponds to parameter variation along the respective path in the parameter plane, and vertical axis – to the dynamical variable x. To produce the distinguishable diagrams, we use a gray coding rule: each time a point fit a definite pixel, a gray code number is increased by 1. In addition, we present respective plots for the Lyapunov exponent; remind that the negative values are associated with torus-attractor, or SNA, and the positive – with chaos.

A road marked (a) corresponds to the Heagy-Hammel scenario [Heagy and Hammel (1994)]. On this path, the parent torus T1 becomes unstable and gives birth to the doubled torus T2 via the torus-doubling bifurcation. Then, the torus T2 grows in width, becomes wrinkled, and touches the parent unstable torus. This is the moment of birth of the SNA. Further motion along this path gives rise to chaos (observe appearance of the positive Lyapunov exponent). The road (b) corresponds to a birth of SNA via intermittency in a course of the transition examined e.g. in Refs. [Prasad *et al.*(1997)] and [Kim *et al.* (2003)]. It looks like a sharp increase of the attractor size, but after the transition the system spends the dominating part of time in a vicinity of the former attractor. The mechanism of the transition is a crisis-like phenomenon consisting in collision of the attractor with a saddle invariant set ("ring-shape sets" in the rational approximation approach, in terminology of Ref. [Kim *et al.* (2003)]). Finally, the road (c) corresponds to the scenario of gradual fractalization of torus-attractor suggested by Kaneko and Nishikawa [Nishikawa and Kaneko (1996)].

We emphasize that the sketched picture appears again and again in smaller scales under magnification by factors δ_1 and δ_2 along the axes of scaling coordinates, with all mentioned elements of the universal pattern of the parameter plane topography. Thus, we conclude again that the TDT point is as an "organizing center" of the whole pattern: any small vicinity of it contains all the main dynamical regimes relevant for the system – tori T1 and T2, SNA, chaos.

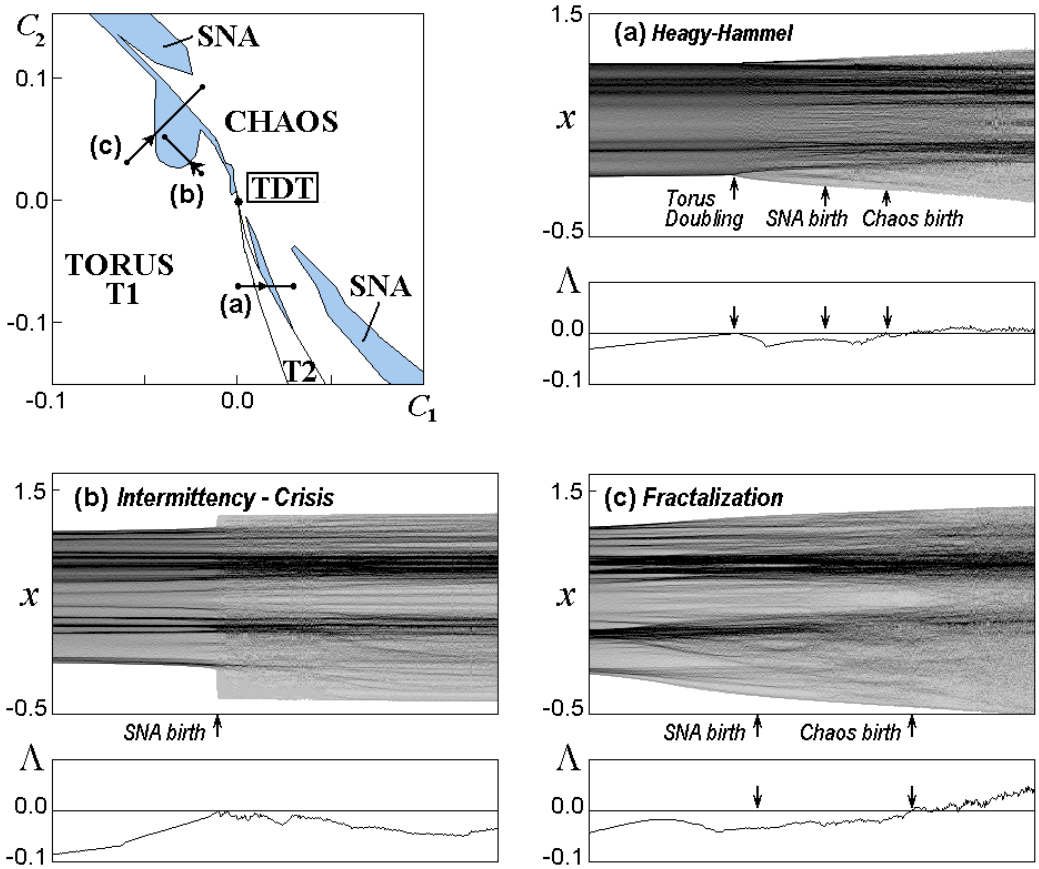

Figure 17: The left top panel is a sketch of the parameter plane topography near the TDT point in scaling coordinates; the areas of torus T1, doubled torus T2, SNA, and chaos are shown. Panels (a), (b), (c) present the bifurcation diagrams (x variable versus parameter) and Lyapunov exponent plots along the paths in the parameter plane marked with the respective letters. The path (a) corresponds to the Heagy-Hammel scenario of birth of SNA (via collision of the wrinkled doubled torus with the parent torus T1), on the path (b) the SNA appears via the intermittency transition examined by Prasad *et al.* and by Kim *et al.*, and on the path (c) via gradual fractalization as suggested by Kaneko and Nishikawa

7 RG analysis of the TCT critical point

In this section, we turn to the RG analysis for the torus-collision terminal point (TCT) [Kuznetsov *et al.* (2000)]. The critical points of this type occur in such models as the driven quadratic map and the driven supercritical circle map. To perform RG analysis, it is more convenient to use the first model, which is simpler. However, for illustrations and classification of dynamical behaviors, the second model is more appropriate, because no divergence of iterations ever happens, in contrast to the first map. In many respects, the schema of reasoning will be very close to that developed in concern with the TDT point in the previous section.

Let us start with a procedure of accurate location of the TCT point in parameter plane of the driven quadratic map

$$x_{n+1} = \lambda - x_n^2 + \varepsilon \cos 2\pi u_n,\ u_{n+1} = u_n + w\,(\mathrm{mod}1). \tag{49}$$

In the unforced map, a tangent bifurcation, that is a collision of a stable fixed point with an unstable partner, takes place at $\lambda = -0.25$ and at $x = -0.5$. This bifurcation corresponds to the lower border of stability interval of λ for the fixed point. For small amplitudes of driving, a fixed point transforms into a smooth closed invariant curve, and the bifurcation consists in a collision of two such curves, one born form a stable, and another form an unstable fixed point, with their subsequent disappearance. At the bifurcation they coincide, and there is a single smooth invariant curve placed entirely in the region $x < 0$ (Fig. 7.18). If we increase the amplitude and go along the bifurcation curve in the parameter plane, an interval occupied by the invariant curve becomes wider, and the maximum value of x on it approaches zero. Finally, it reaches zero. This event corresponds to the terminal point of the bifurcation curve, the TCT critical point. As we stay on the bifurcation curve, a typical orbit on the torus is just at the instability threshold. However, a touch with zero implies that a superstable orbit appears among other trajectories on the torus, which contains the parabola maximum x=0.

For a rational frequency $w_m = F_{m-1}/F_m$, instead of the invariant curve, we get a cycle of period F_m. It depends on the initial phase u_0, which may be regarded as an additional parameter. Let us require the set of orbits with different initial phases, which approximates the torus, to touch $x = 0$. It means that at some phase $u_0 = u^0$ there exists a cycle of period-F_m starting from $x = 0$, and the derivative dx/du_0 vanishes. (Zero derivative means a touch of the line $x = 0$ by the approximate torus: nearby orbits do not

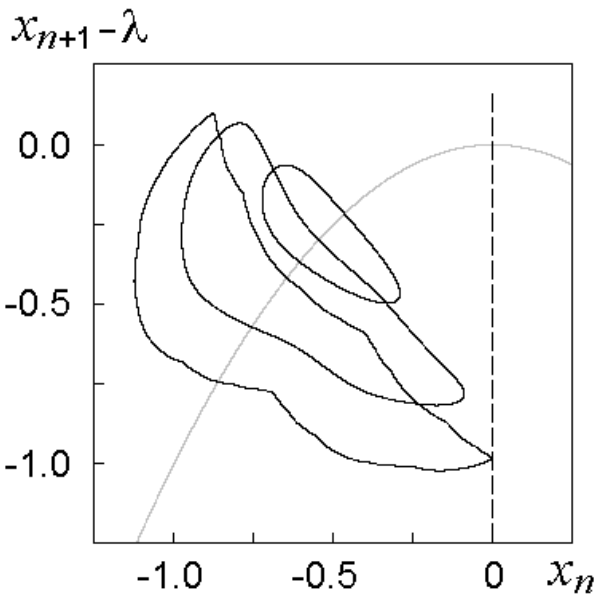

Figure 18: The invariant curves at the torus collision bifurcation: smooth tori for $\varepsilon = 0.4$, $\lambda = -0.22696$ and $\varepsilon = 0.8$, $\lambda = -0.15716$, and the critical torus at ε_c, λ_c. The plot is drawn with a shift of the vertical coordinate by λ, so that the graph of the quadratic map has the same form for all parameter values. The critical torus touches the line $x = 0$

intersect this line.) Simultaneously, we demand the collision bifurcation to occur, i.e. the maximum of the Floquet multiplier equals 1 for the period-F_m cycle at some other initial phase $u_0 = u^1$.

At each level of the rational approximation, we can estimate numerically λ and ε, and phases u^0 and u^1, at which the conditions are satisfied. In Table 7.2 the numerical data are summarized. Observe evident convergence under increase of the order of approximation. The limits for λ and ε determine location of the TCT point in the parameter plane. Our best result obtained from computations with high accuracy (60-digit precision, at levels of Fibonacci numbers up to 514229...3524578) is

$$\lambda_c = -0.09977122895,\ \varepsilon_c = 1.01105609099,\ \text{and}\ u_c = 0.53372941325, \quad (50)$$

where u_c is a common limit for the phase sequences u^0 and u^1.

Table 2: Numerical data for the torus collision terminal point in rational approximations for the driven quadratic map (49)

w_m	λ	ε	u^0
8/13	-0.106863851767	0.989187201082	0.505473909903
13/21	-0.104845946249	0.993122021583	0.551881855417
21/34	-0.102132053793	1.003742152765	0.523043122989
34/55	-0.101301679580	1.005940852360	0.540532546847
55/89	-0.096519589548	1.008703220940	0.529671825167
89/144	-0.096227513110	1.009565266966	0.536295837724
144/233	-0.096003370260	1.010319151502	0.532185483229
233/377	-0.099907304210	1.010615844857	0.534709662240
377/610	-0.099842405051	1.010828952123	0.533141299658
610/987	-0.09981191332417	1.01096505020861	0.53409804003715
987/1597	-0.09979689883669	1.01098675212306	0.53350525381290
1597/2584	-0.09978341968243	1.01101690728124	0.53386947751449
2584/4181	-0.09977779656842	1.01103504807250	0.53364394312993
4181/6765	-0.09977488690490	1.01104434510749	0.53378268847958
6765/10946	-0.09977321340337	1.01104972857703	0.53369681588723

TCT critical point occurs also in the forced supercritical circle map

$$\begin{aligned} x_{n+1} &= x_n + r - (K/2\pi)\sin 2\pi x_n + \varepsilon\cos(2\pi u)\,(\mathrm{mod}1), \\ u_{n+1} &= u_n + w \ \ (\mathrm{mod}1). \end{aligned} \tag{51}$$

'Supecritical' means that parameter K is larger then 1, and the mapping for x in non-invertible. For definiteness, we fix $K = 2.5$. Locally, near the extremum at $x^0 = \arctan(\sqrt{K^2-1})/2\pi$, the right-hand function in the equation looks similar to the parabola map, so it is natural that the same type of criticality takes place. The condition is that an invariant curve at the threshold of collision bifurcation touches x^0. In Table 7.3 we present numerical data for the circle map at rational approximations of the frequency parameter (analogous to those in Table 7.2 for quadratic map). Observe convergence to definite limits determining location of the TCT point. The best estimates obtained from computations with 20-digit precision up to Fibonacci numbers 46368...317811 yield

$$b_c = 0.377866239,\ \varepsilon_c = 0.132566321,\ u_c = 0.284109286. \tag{52}$$

Table 3: Numerical data for the torus collision terminal point in rational approximations for the driven circle map (51) at $K = 2.5$

w_m	λ	ε	u^0
8/13	0.37881706168188	0.12963650656581	0.25582995050593
13/21	0.37853943959631	0.13019323399852	0.30220519948417
21/34	0.37818176558166	0.13158976184330	0.27342021471748
34/55	0.37806966405365	0.13188906990693	0.29089396540962
55/89	0.37796607502727	0.13225282828857	0.28005156151726
89/144	0.37796680039671	0.13236878805042	0.28666996177228
144/233	0.37789716819380	0.13246827351501	0.28256543113078
233/377	0.37788430788852	0.13250795751162	0.28507911784015
377/610	0.37787571332547	0.13253613129985	0.28352121995658
610/987	0.37787164279323	0.13254894376094	0.28447737339461
987/1597	0.37786912162019	0.13255711167252	0.28388514644255
1597/2584	0.37786785844262	0.13256112439438	0.28424919682601

Now, to reveal nature of solution of the RG equation (6) associated with the TCT criticality, one can try to compute terms of the functional sequence $g_m(X,Y)$ via iterations of a model map at the critical point. At this place, it is more convenient to deal with the quadratic map. Given a sufficiently large Fibonacci number F_m, we first set the initial condition $x_0 = 0$, $u_0 = u_c$ and from iterations of the map get $x_{Fm} = x^0_{Fm}$. Then, to obtain $g_m(X,Y)$ for some particular X and Y, we again iterate the map (49), but with initial conditions $x_0 = x^0_{Fm}X, u_0 = u_c + (-w)^m Y$. After F_m iterations we obtain the resulting x_{Fm} and set $g_m(X,Y) = x_{Fm}/x^0_{Fm}$. Such computations show that the sequence of functions tend to a definite limit, $g_m(X,Y) \to g(X,Y)$. This is a fixed point of the RG equation (6), i.e.

$$g(X,Y) = \alpha^2 g(\alpha^{-1} g(X/\alpha,\, -wY),\, w^2 Y + w). \tag{53}$$

Here the scaling factor α, as estimated from the computations, is $\alpha \cong x^0_{Fm}/x^0_{Fm+1} \cong 1.71$. (In fact, the convergence is rather slow, and to get really good approximation it is necessary to use either sufficiently large Fibonacci numbers and/or to reveal and account character of the convergence; see [Kuznetsov *et al.* (2000)] for some details.)

The next step is to obtain an accurate numerical solution of the functional equation (6).

One possible approach is to approximate the function $g(X,Y)$ by a finite polynomial containing odd and even powers of Y and even powers of X, and to search numerically for a set of coefficients of this polynomial satisfying Eq.(6) with the best possible accuracy. A straightforward realization of this idea appears not to be feasible, and some tricks are necessary. First, we select a restricted domain of the definition for the function g in the (X,Y) plane. The condition is that for any point (X,Y) of this domain D the points $(X/\alpha, -wY)$, and $(\alpha^{-1} g(X/\alpha, -wY), w^2 Y + w)$ (see the right hand part of Eq. (53)) belong to D. From the approximate data for $g(X,Y)$, one can check that the domain

$$D : \{ -0.1 + 0.9Y < |X| < 0.1 + 0.9Y, -w < Y < 1\} \tag{54}$$

is appropriate. For representation of the function in D an expansion in orthogonal Chebyshev polynomials over two arguments was applied, and by a Newton method the coefficients of this expansion were computed. As initial guess, a function obtained numerically from iterations of the quadratic map at the TCT point was used. A final result is a solution of Eq. (6) found with

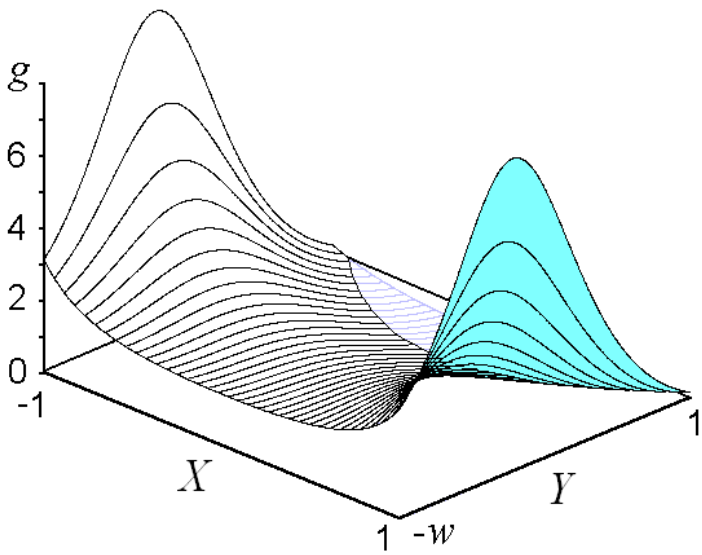

Figure 19: 3D plot of the function $g(X, Y)$ representing the fixed point of the RG equation associated with the TCT critical point

precision of order 10^{-7}. To compute the function outside the region D, one has to use functional equation (6) and construct appropriate compositions of the numerically obtained function under requirement that the argument values, at which the computations are performed, relate to D. A plot of the fixed-point function is shown in Fig.7.19. The accurate estimate for the scaling factor obtained from the solution of the functional equation is

$$\alpha = 1.7109605. \tag{55}$$

Up to a characteristic scale, the function $g(X, Y)$ determines asymptotically the evolution operators for F_m iterations of the original driven quadratic map at the TCT critical point. It implies presence of similarity of the dynamics on the respective time scales and scaling regularities.

One step of the RG procedure corresponds to increase of time scale by factor $\tau_m = F_{m+1}/F_m$, asymptotically $\tau = 1/w = 1.618034$, and decrease of scales for variables $X = x$ and $Y = u - u_c$ by factors $\alpha = 1.7109605$ and $\beta = 1/(-w) = -1.618034$, respectively.

From Fig. 7.18 one can observe that attractor at the TCT critical point looks as a fractal-like curve. To reveal its scaling property, let us consider a plot of the critical attractor in coordinates (u, x). If we rescale $X = x$

and $Y = u - u_c$ by factors α and β, respectively, then the dynamics is expected to be similar, but with increase of a characteristic time scale by τ. Hence, the curve representing the critical attractor must be invariant under this transformation. Figure 7.20 demonstrates that indeed this is the case: The picture inside the selected box reproduces itself under subsequent magnifications (with inversion in respect to the horizontal axis, due to the negative scaling factor). This scaling property near the origin implies that the critical curve must behave locally as $x \propto |\Delta u|^{\kappa}$ with $\kappa = \log\alpha/\log|\beta| \cong 1.117$. The power is close to one, so visually the curve looks like broken at the point of singularity. Singularities of the same type will be present also at all points, to which the origin is mapped under subsequent iterations. Due to ergodicity of the quasiperiodic motion, this is a dense set of points over the invariant curve, and this explains the fractal-like shape. In fact, the singularity is weak: κ is slightly larger than 1. As follows, the invariant curve is differentiable, although not twice differentiable.

Fig.7.21 presents analogous verification for the scaling property of the critical attractor at the TCT point of the driven circle map. Here the main singularity is placed at $x^0 = \arctan(\sqrt{K^2-1})/2\pi$. This is a minimum of the right-hand function (in contrast to the considred logistic map, which has a maximum); on this reason the picture is upside down.

Before discussion of the scaling regularities intrinsic to a vicinity of the TCT point we have to remind that this is a point of meeting of bifurcation lines, one corresponds to the smooth tori collision, and another to the intermittent transition (see Sec.7.3). After crossing one of these bifurcation borders, the localized attractor disappears, but in the part of phase space of its former existence the trajectories travel for very long time: the closer to the bifurcation, the larger the characteristic time. From the global point of view, there are two possibilities. First, it may occur that after the passage through the mentioned part of phase space the orbit never returns back (this is the case of quadratic map, where the divergence takes place). Alternatively, it may happen that a re-injection mechanism exists, due to which the orbit returns into that part of phase space again and again (this is the case for the circle map). Then, after crossing the bifurcation borders of the area of torus stability one will observe transition to SNA or to chaos via intermittency. These dynamical regimes, however, are not bounded in the domain of former existence of the localized attractor, and, hence, the conclusions from the analysis in terms of linearized RG equation is not applicable for them, at least in a straightforward manner. (Here an analogy

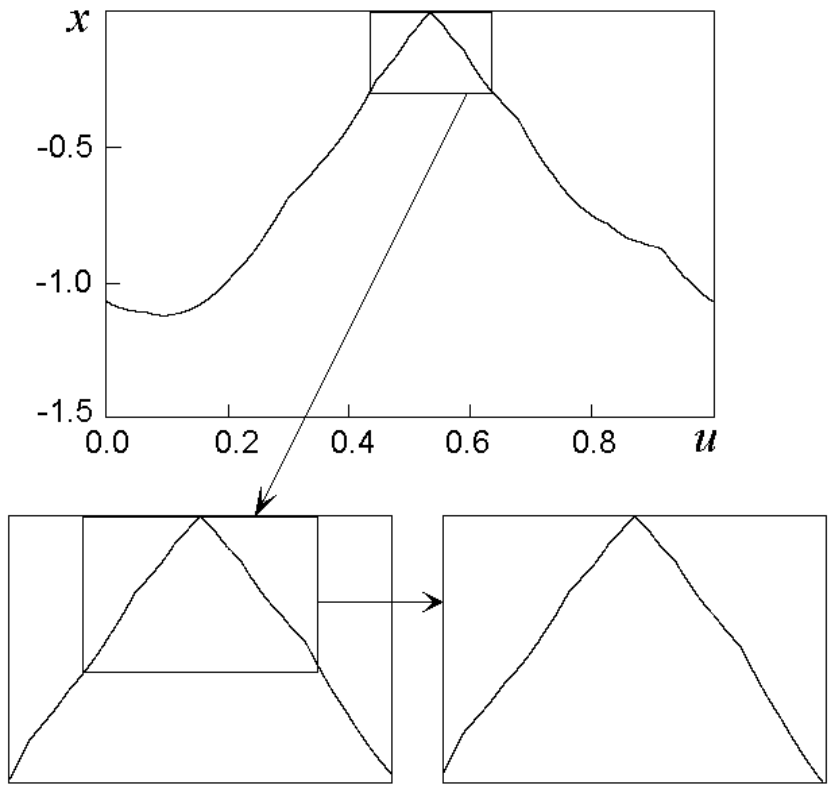

Figure 20: Scaling of the critical torus for the driven quadratic map in the phase plane (u, x) at the TCT point. The top panel shows the whole picture, the next one presents the enlargement of the selected box, and the last – enlargement of the box from the previous one, under magnification by $\alpha = 1.7109$ for the vertical axis, and $\beta = (-w)^{-1} = -1.6180$ for the horizontal axis. Negative value of β means that the magnification is accompanied by reflection along the horizontal direction

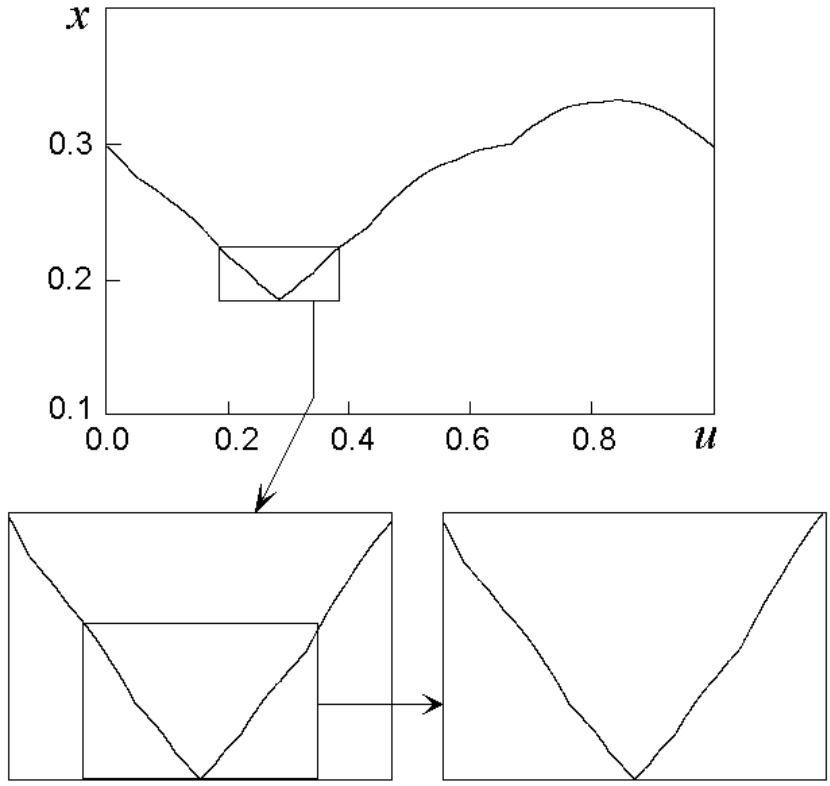

Figure 21: Scaling of the critical torus for the driven circle map in the phase plane (u, x) at the TCT point. The top panel shows the whole picture, the next one presents the enlargement of the selected box, and the last – enlargement of the box from the previous one, under magnification by $\alpha = 1.7109$ for the vertical axis, and $\beta = (-w)^{-1} = -1.6180$ for the horizontal axis

may be useful with the analysis of the classic intermittency of Pomeau and Manneville [Pomeau and Manneville (1980)], where the RG approach relates only to laminar stages, while the properties for the turbulent bursts are postulated, as an additional component of the theory.) Having in mind these restrictions, we assume further that the second alternative takes place, and turn now to analyses of the perturbations for the fixed-point solution of the RG equation.

Let us substitute $g_m(X,Y) = g(X,Y) + \delta^m h(X,Y)$ into Eq.(6), and in the first order in h get the eigenvalue problem for the linearized functional equation

$$\begin{aligned} \delta^2 h(X,Y) = \; & \alpha\delta g'(\alpha^{-1}g(X/\alpha,\, -wY),\, w^2Y + w)h(x/\alpha,\, -wY) \\ & +\alpha^2 h(\alpha^{-1}g(X/\alpha,\, -wY),\, w^2Y + w). \end{aligned} \tag{56}$$

As we locate the TCT point tuning two free parameters, we expect to have two relevant eigrnvalues, namely, δ_1 and δ_2, which are larger than 1 in modulus. Then, asymptotic behavior of the infinitesimal perturbation to the fixed-point solution will contain the corresponding two eigenvectors and for the perturbed evolution operator we have to write

$$g_k(X,Y) \cong g(X,Y) + C_1(\varepsilon,b)\delta_1^k h_1(X,Y) + C_2(\varepsilon,b)\delta_2^k h_2(X,Y). \tag{57}$$

Here C_1 and C_2 are coefficients, which depend on parameters of the original map and vanish at the critical point.

Numerical solution of the linearized equation (56) is based on approximation of the function $h(X,Y)$ by finite Chebyshev polynomial expansions, with substitution of $g(X,Y)$ and α, which are already computed. On this way, we reduce the functional equation to an eigenproblem for a finite matrix, which allows solution by standard methods of linear algebra. After excluding the eigenvalues, which are less than 1 in moduls, those associated with infinitesimal variable changes, and with departures from the commutative subspace, only two relevant eigenvalues remain in the rest:

$$\delta_1 = 3.600810..., \quad \delta_2 = 1.828329... \tag{58}$$

To state the basic scaling property, let us suppose that we consider a dynamical regime at a point (ε, b), which corresponds to some values of the coefficients $C_1 = C_1^0$ and $C_2 = C_2^0$ in (57). If we now take such point (ε', b') that the coefficients will be equal to $C_1 = C_1^0/\delta_1$ and $C_2 = C_2^0/\delta_2$, then the

renormalized evolution operator for F_{m+1} iterations at the new point will be the same as the evolution operator for F_m iterations at the old point (see (57)).

For convenience, we could introduce a special local coordinate system (*scaling coordinates*) near the critical point; for this we simply regard C_1, C_2 as the coordinates. Then, a simultaneous scale change along the coordinate axes by factors δ_1 and δ_2, respectively, corresponds to the condition of similarity of the evolution operators. Unfortunately, we do not know explicit expressions for C_1, C_2 via parameters of original map, so the problem has to be resolved numerically, with sufficient accuracy.

Let us construct an ersatz, the coordinate system (c_1, c_2) with origin at the critical point. One coordinate axis, corresponding to larger scaling factor δ_1, may be directed almost arbitrarily. A shift along this direction has to contribute in the coefficient C_1 in (57); so, the only condition is that it must be transversal to a curve on the parameter plane defined by an equation $C_1(\varepsilon, b) = 0$. In contrast, the second coordinate must be defined carefully, because contribution into the senior eigenvector should be excluded. For this, the curve $C_1(\varepsilon, b) = 0$ in new coordinates has to be a coordinate curve, along which the value of c_2 is measured. One may try to search for explicit expression via Taylor expansion, say in the form

$$\Delta\varepsilon = c_2,\ \Delta b = Ac_2 + Bc_2^2 + Cc_2^3 + \dots. \tag{59}$$

However, we are within ours rights to account a finite number of terms in this expansion. Suppose we consider a sequence of pictures of the parameter plane near the critical point in smaller and smaller scales, namely $c_1 \propto \delta_1^{-k}$ and $c_2 \propto \delta_2^{-k}$. If we neglect a Taylor coefficient at c_2^m, the deflection from the proper coordinate curve will behave as δ_2^{-mk}, the respective contribution into the senior eigenvector in the evolution operator (57) well be of order $\delta_2^{-mk}\delta_1^k$. In accordance with our numerical data for the eigenvalues, we have $\delta_2 < \delta_1$ and $\delta_2^2 < \delta_1$, but $\delta_2^m > \delta_1$ for $m \geq 3$. Hence, it is sufficient to retain in (59) only linear and quadratic terms.

In a spirit of the above discussion, for definition of the scaling coordinates near the TCT critical point we can use the following ansatz

$$\varepsilon = \varepsilon_c + c_2,\ \lambda = \lambda_c - c_1 + A_q c_2 + B_q c_2^2. \tag{60}$$

The coefficients may be found if the torus-collision bifurcation curve is computed: This curve has to coincides with the coordinate curve c_1=0; coefficient

A_q is connected with the slope of the bifurcation curve at the TCT point in the original coordinates (ε, λ), while B_q is connected with its curvature. Accurate computations yield for the quadratic map

$$A_q{=}0.3117076,\ B_q{=}0.2819.$$

Analogously, for the circle map we set

$$\varepsilon = \varepsilon_c + c_2,\ b = b_c + c_1 + A_c c_2 + B_c c_2^2. \tag{61}$$

where

$$A_c = -0.3121848, B_c = -2.047. \tag{62}$$

If the dynamical regime that we deal with takes place completely in the domain of phase space, in which the RG procedure is valid, then a nature of the dynamics should be similar at (c_1, c_2) and $(c_1/\delta_1,\ c_2/\delta_2)$, and the both regimes may differ only by characteristic time scale, which is larger at the second point by factor $\tau = 1/w$. Moreover, quantitative characteristics of both regimes are expressed one via another by trivial relations. Say, the Lyapunov exponents are connected as $\Lambda(\varepsilon', b') \cong \Lambda(\varepsilon, b)/\tau$. Fore sure, all this is true for the localized attractors before the bifurcation of smooth collision or intermittency birth.

In Fig.7.22 we present the Lyapunov charts of dynamical regimes for our two models using gray scale coding. A small fragment selected near the TCT critical point with borders going along coordinate lines of the scaling coordinate system, and is shown separately. Smaller fragment of the last picture is magnified several times by factors δ_1 and δ_2 along the horizontal and vertical axes, respectively, to demonstrate similarity of the observed topography. Depicting the diagrams under subsequent steps of magnification, we change the rule of the gray scale coding accounting the rule of renormalization of the Lyapunov exponent. Observe nice coincidence of the plots at subsequent stages of the magnification.

Let us summarize, what can we say about arrangement of the dynamical regimes near the TCT point on a basis of the stated scaling properties of the evolution operators. In the top panel of Fig.7.23 we reproduce a sketch of the parameter plane near the TCT point in scaling coordinates. Other panels present the bifurcation diagrams and Lyapunov exponent plots corresponding to the paths in the parameter plane marked (a) and (b). The most notable feature of the picture is that at the TCT point two bifurcation curves meet. One, which goes along the coordinate line $c_1 = 0$, is the line of smooth tori

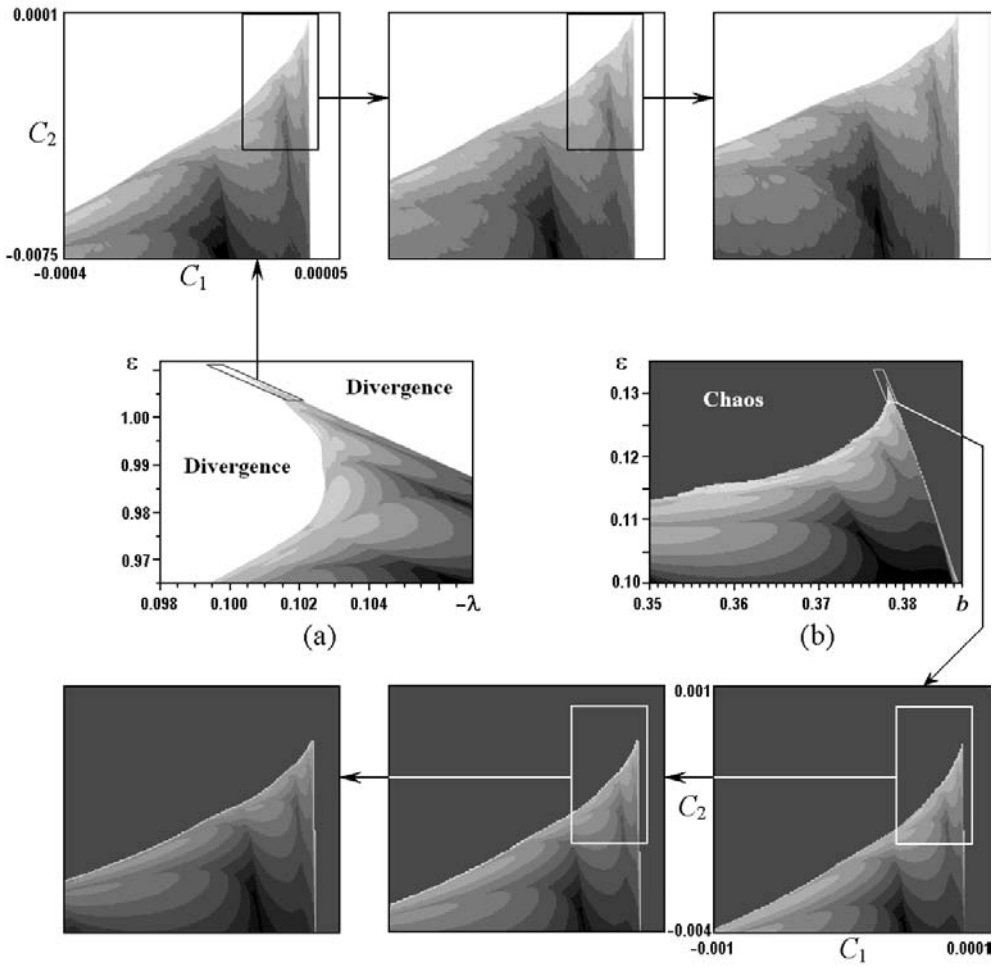

Figure 22: Demonstration of the scaling properties on the parameter plane near the TCT critical points. We plot the Lyapunov exponent for the quadratic map (a) and circle map (b) using a gray scale. For clarity of presentation, only the region of negative exponents is resolved. The main panels (a) and (b) show the Lyapunov charts in the original coordinates on the parameter planes. The insets are depicted in scaling coordinates under successive magnifications: the horizontal scale is increases by factor $\delta_1 \approx 3.65$, and the vertical scale by the factor $\delta_2 \approx 1.81$. The level of the Lyapunov exponent are coded by the gray scale, from light (positive values) to dark (negative values). The coding rule from picture to picture is redefined according to the scaling relation expected to the Lyapunov exponent: the border values for each gray tone are decreased by factor $\tau = 1.61803$

collision, and another, the top curve border, corresponds to an intermittent transition from localized to delocalized attractor. From the stated scaling law, it is easy to derive a relation for this curve, it must obey the power law

$$c_2 \cong \text{const} \cdot |c_1|^\gamma,\ \gamma = \log\delta_2/\log\delta_1 = 0.470981\ldots \tag{63}$$

On the road (a), the observed scenario of the onset of complex dynamics involves bifurcation of smooth collision of stable and unstable tori, with their coincidence at the bifurcation, and with subsequent disappearance. After that (in the presence of the re-injection mechanism, like in the driven circle map), the result is the onset of intermittent chaotic regime. On the road (b) the intermittent transition, as observed in computations, occurs at the moment of a touch of the attractor with an unstable invariant curve. At the transition the Lyapunov exponent is negative, so, the only possibility is that the arising intermittent regime corresponds to SNA. It is not clear does the localized attractor becomes strange (fractalized) before the intermittent transition takes place, or it remains a smooth (although wrinkled) torus up to the transition. It is also possible that both alternatives occur at different parts of the bifurcation border. It is clear, however, that the complex form of the attractor at the transition is linked with the fact that the map is non-monotonic in the region of the attractor disposition (the extremum of the map belongs to the domain of the attractor). As to the unstable invariant curve, it is placed completely in the interval of monotonic behavior of the map, and, as seen from computations, it remains smooth up to the moment of bifurcation and further. As observed, the regimes of intermittent SNA occupy a very narrow strip in the parameter plane along the chaos border. (At subsequent magnification of the picture in accordance with scaling relations, this strip becomes yet more and more narrow, i.e. its width apparently does not obey the scaling law.)

8 RG analysis of the TF critical point

In the map $x_{n+1} = x_n/(1-x_n)+b$, as we increase the parameter b, a tangent bifurcation takes place. The bifurcation consists in collision of a stable fixed point and an unstable one, with their subsequent disappearance. After this event, a narrow 'channel' remains in the region of former existence of the pair of the fixed points, through which the orbits travel for a long time. The closer to the bifurcation point, the larger is the passage time. This picture is a key

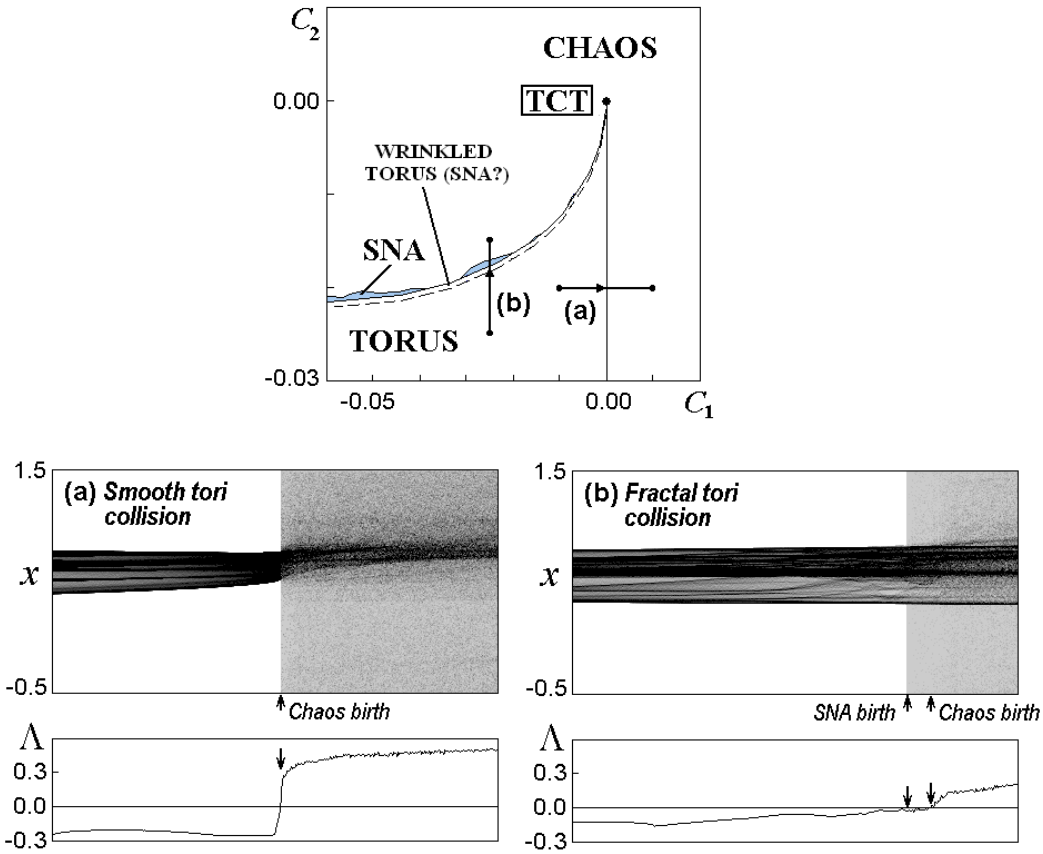

Figure 23: The top panel is a sketch of the parameter plane topography near the TCT point in scaling coordinates in a case of the excluded divergence, as it appears, say, in the driven circle map. The areas of torus, SNA, and chaos are shown. Panels (a) and (b) present the bifurcation diagrams (x variable versus parameter) and Lyapunov exponent plots along the paths in the parameter plane marked with the respective letters. The path (a) corresponds to collision of smooth stable and unstable tori with their subsequent disappearance and intermittent transition to chaos. On the path (b) the bifurcation consists in a fractal collision of a smooth unstable torus and an attractor (a wrinkled stable torus or an SNA), with a birth of SNA, which exists in a very narrow strip in the parameter plane; then the transition to chaos follows

element of the transition to intermittent dynamics suggested by Pomeau and Manneville [Pomeau and Manneville (1980)]. Another necessary element of the intermittency is presence of the mechanism of re-injection: after the travel through the channel the orbit should return to repeat this passage again and again.

Adding a quasiperiodic force with the golden mean frequency, we get a map

$$x_{n+1} = x_n/(1-x_n)+b+\varepsilon\cos 2\pi u_n,\ u_{n+1} = u_n + w\,(\bmod 1),\ w = (\sqrt{5}-1)/2. \tag{64}$$

In this model, at small amplitudes ε a transition is very similar to the tangent bifurcation, but, instead of the fixed points, the participants are two smooth invariant curves, one stable and another unstable. In a course of the transition, they meet with complete coincidence and annihilate. Then, a region of long-time travel of orbits appears at the place of the former existence of the invariant curves. (The models of form (64), or equivalent, up to variable changes, were suggested and discussed e.g. in Refs. [Ketoja and Satija (1997a)], [Negi and Ramaswamy (2001)], [Datta *et al.* (2003)].)

At larger ε, the nature of the transition becomes drastically different. At the bifurcation the invariant curves neither coincide, nor remain smooth. What observed is formation of a set of narrow sharp 'spikes' on the invariant curves, and mutual touch of them by these spikes. Due to ergodicity of the quasiperiodically forced motion, the spikes, in fact, occupy a dense set on the invariant curve. Obviously, the object we deal with at the bifurcation, is a fractal, and the event is called the fractal tori collision.

The both mentioned situations are clearly separated at some critical amplitude of driving; in the model (64) this separation occurs precisely at $\varepsilon = 2$. This special point on the bifurcation border of touch of the stable and unstable invariant curves is the *TF critical point* ('torus fractalization'.) [Kuznetsov (2002)].

To start, let us discuss a procedure of accurate location of the TF critical point.

The first intriguing question is: Why does it corresponds exactly to $\varepsilon = 2$? The answer may be obtained on the following way. With a substitution $x_n = 1 - \psi_n/\psi_{n-1}$ the equation (64) transforms into the *Harper equation*

$$\psi_{n+1} + \psi_{n-1} + (-2 + b + \varepsilon\cos 2\pi(nw+u))\psi_n = 0, \tag{65}$$

known in solid-state phusics in the context of wave propagetion in a one-dimensional model of a quasicrystall (Harper equation) [Harper, 1955], [Suslov (1982)], [Ketoja and Satija (1997b)]. In this interpretation, ψ_n is a wave function, n is index on a spatial discrete lattice, ε is amplitude of spatially quasiperiodic perturbation, and b is an eigenvalue assotiated with frequency, or energy in the quantum-mechainical problem. At small ε, the dominaiting type of behavior corresponds to propagating waves, with exception of narrow forbiding frequency bands. At large ε, the wavefunctions are localized, no propagating. In accordance with argument of André and Aubry [André and Aubry (1980)], the transition from delocalized to localized states occurs just at $\varepsilon = 2$. Namely, application of the Fourier-like transformation

$$\phi_k = \hat{F}\psi_n = \sum_{n=-\infty}^{n=\infty} \psi_n e^{2\pi i n k w} \tag{66}$$

to Eq.(65) yields a relation of similar form

$$\phi_{k+1} + \phi_{k-1} + (-2 + b' + \varepsilon' \cos 2\pi(nw + u))\phi_k = 0, \tag{67}$$

where

$$\Omega' = 2 + 2(\Omega - 2)/\varepsilon,\ \varepsilon' = 4/\varepsilon. \tag{68}$$

Localization of the wave function impies delocalization of its transform and vice versa. So, the transition must occur at $\varepsilon = 2$, which corresponds to a fixed point of the equation for ε. It may be proven that the localized solutions of the Harper equation correspond to orbits of the original fractional-linear map asymptotic at $t \to \infty$ to a localized attractor, and at $t \to -\infty$ to a localized unstable invariant set. Delocalized solutions of the Harper equation correspond to orbits, which depart in a course of the motion from the main branch of the map ($x < 1$).

Next, to obtain an accurate estimate for the critical value of b, we may turn to computations based on rational approximations of the frequency parameter by ratios of Fibonacci numbers, $w_m = F_{m-1}/F_m$. At frequency w_m the driving is periodic, and the transition consists in the tangent bifurcation of the period-F_m orbit. It is a collision of a stable cycle with an unstable one, and their Floquet multipliers tend to 1 at the bifurcation. The bifurcation occurs at some b dependent on the initial phase u_0. As observed, the minimal value of b, at which the bifurcation takes place, corresponds to u_0=0, the situation of symmetry of the Harper equation in respect to inversion of u at the origin. So, we consider a symmetric solution, for which

$\psi_1 = \psi_{-1} = \frac{1}{2}(-2 + b + \varepsilon)\psi_0$, and, hence,

$$x_0 = (b + \varepsilon)/(b + \varepsilon - 2). \tag{69}$$

In the computations we set $\varepsilon = 2$, $w = w_m$, put the initial conditions $x = x_0$ and $u = 0$, and try to ajust the only unknown parameter b to have a cycle of period F_m, i.e., to get $x_{Fm} = x_0$. Results of such computations are presented in Table 7.4. One can observe evident convergence of the sequence of b values. So, we conclude that the critical point is located at

$$(\varepsilon,\, b)_{TF} = (2,\, -0.597515185\ldots). \tag{70}$$

Table 4: Numerical data for the values of b in the map (64) corresponding to the cycle collision at $u = 0$ for the critical amplitude $\varepsilon = 2$

w_k	b
8/13	−0.5989496730498198
13/21	−0.5993564164969890
21/34	−0.5975700101088623
34/55	−0.5977371349948819
55/89	−0.5975077597293093
89/144	−0.5975427315196966
144/233	−0.5975125430279679
233/377	−0.5975187094612125
377/610	−0.5975146415227064
610/987	−0.5975156490874847
987/1597	−0.5975150899617102
1597/2584	−0.5975152478940331
2584/4181	−0.5975151698106684
4181/6765	−0.5975151939749183
6765/10946	−0.5975151829388339
10946/17711	−0.5975151865779841

To find out of what kind a solution is of the RG equation associated with the FT critical point, we may try to compute the functions g_k from direct iterations of the map (64) in the same way as in the previously analyzed

critical situations. A straightforward attempt fails because the variable x in the original map does not correspond to that in the RG equation. It is necessary to perform preliminary a variable change; an appropriate new coordinate may be defined as a distance from the invariant curve $x = \xi(u)$ at the transition, namely,

$$X \propto x - \xi(u), \quad \xi(u) = x_c + Pu + Qu^2. \tag{71}$$

Here $x_c = (b_c + 2)/b_c = 2.34719526$, as follows from Eq.(69) with substitution $\varepsilon = 2$, $b = b_c$. P and Q are coefficients estimated numerically via the first and the second derivative for the invariant curve: $P = (\partial\xi/\partial u)_{u=0} = -5.92667$ and $Q = \frac{1}{2}\left(\partial^2\xi/\partial u^2\right)_{u=0} = 210.629$.

Now the procedure consists in the following. (i) For given X and u define the initial conditions for iterations of the map (64): $x = X\alpha^{-k} + x_c + Pu_c + Qu^2$, $u = U$ with $\beta = -1/w$, α is empirically selected constant, approximately, 2.89. (ii) Produce F_k iterations of the map (64). (iii) Return to variable X by the inverse relation $X = \alpha^k\left(x - x_c + Pu + Qu^2\right)$.

The computations show that at k sufficiently large the resulting functions clearly become independent of k, i.e. we deal with a fixed point of the RG equation (6), see Fig.7.24.

To continue, we note that due to the fractional-linear nature of the map, the functions obtained at subsequent steps of the RG transformation (6) will will be fractional-linear too. The same is true for the limit fixed-point function. Therefore, we may search for solution in a form

$$g(X, u) = (a(u)X + b(u))/(c(u)X + d(u)), \tag{72}$$

where a, b, c, d are some functions of u. Without loss of generality, we require them to satisfy additional conditions $a(u)d(u) - b(u)c(u) \equiv 1$, and $c(0) = 1$. Substituting (72) into (6) we arrive at the fixed-point RG equation in terms of the functions a, b, c, d:

$$\begin{bmatrix} a(u) & b(u) \\ c(u) & d(u) \end{bmatrix} = \begin{bmatrix} a(w^2u + w) & \alpha^2 b(w^2u + w) \\ \alpha^{-2}c(w^2u + w) & d(w^2u + w) \end{bmatrix} \cdot \begin{bmatrix} a(-wu) & \alpha b(-wu) \\ \alpha^{-1}c(-wu) & d(-wu) \end{bmatrix}. \tag{73}$$

The solution was found numerically, and the coefficients of polynomial expansions for $a(u)$, $b(u)$, $c(u)$, $d(u)$ are listed in Ref. [Kuznetsov (2002)] (see also web page

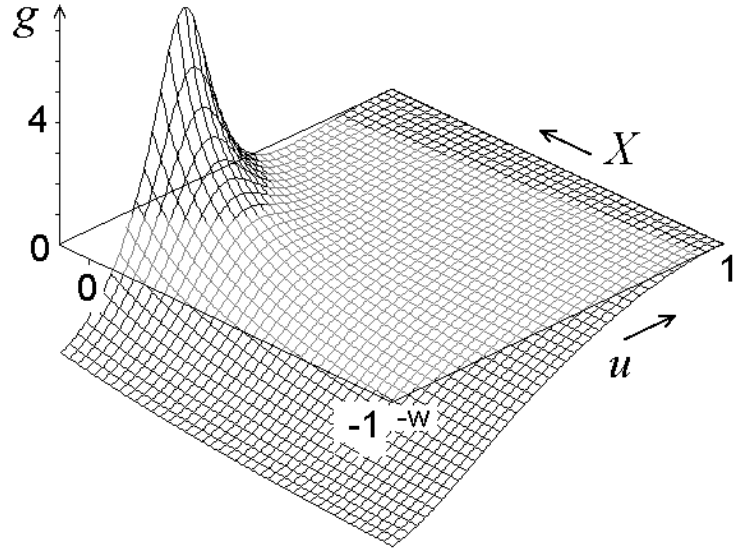

Figure 24: 3D plot of the function $g(X, u)$ representing the fixed point of the RG equation associated with the TF critical point

http://www.sgtnd.narod.ru/science/alphabet/eng/goldmean/tf.htm).
The factor α was also computed, so

$$\alpha = 2.890053525\ldots \text{ and } \beta = -w^{-1} = 1.6180339\ldots \tag{74}$$

These two constants are responsible for the scaling properties of the critical attractor. In Fig.7.25 the left panel shows the portrait of the attractor in the conventional $(u,\, x)$-plane, which looks like a wrinkled curve. A selected curvilinear quadrilateral area has the sides coinciding with coordinate lines of the local scaling coordinate system (71). The interior of this quadrilateral is shown separately in the top right panel in the scaling coordinates. Observe self-similarity of the pictures: each the next, drawn with magnification by factors α and β along the horizontal and vertical axes, respectively, reproduces all fine details of the previous one with excellent accuracy.

Numerical solution of the eigenvalue problem (8) for the fractional-linear fixed point yields two relevant eigenvalues

$$\delta_1 = 3.134272989\ldots,\ \delta_2 = 1.618033979\ldots \tag{75}$$

They determine the scaling properties of the evolution operators near the critical point. If we depart from the critical point along the bifurcation

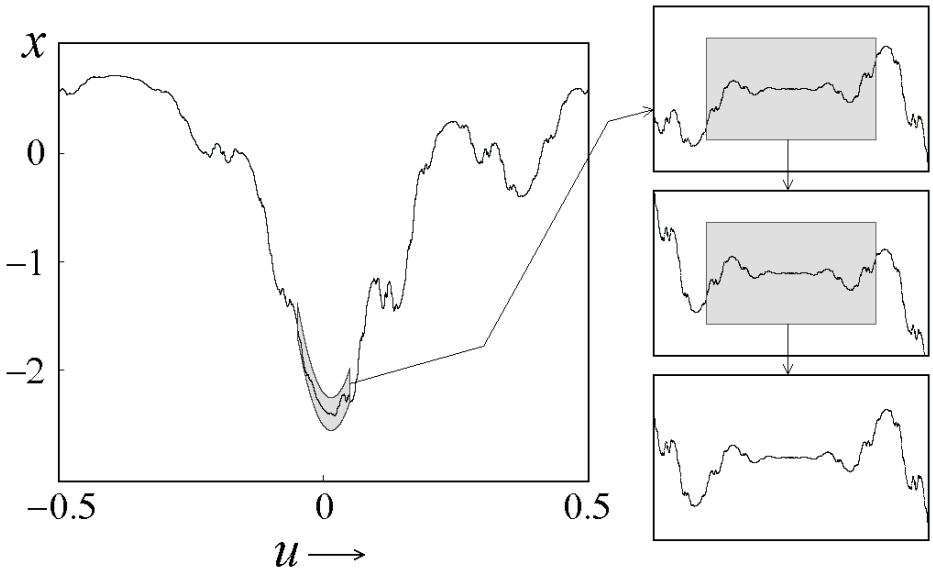

Figure 25: Attractor of the forced fractional-linear map at the TF critical point (the left panel) and illustration of the basic local scaling property: the structure depicted in scaling coordinates reproduces itself under magnification with factors $\alpha = 2.89005$ and $\beta = -1.61803$ along the vertical and the horizontal axes, respectively

curve, the first eigenvector does not contribute; the relevant perturbations are associated with δ_2. If we choose a transversal direction, say, along the axis b, the perturbation of the first kind appears.

In the case under consideration we have $\delta_1 > \delta_2$ and $\delta_1 > \delta_2^2$, but $\delta_1 < \delta_2^3$, so quadratic terms must be taken into account in the parameter change. The scaling coordinates (C_1, C_2) are linked with parameters of the original map as

$$b = b_{TF} + C_1 - 0.64938C_2 - 0.33692C_2^2,\ \varepsilon = 2 + C_2. \tag{76}$$

To examine scaling associated with the nontrivial constant δ_1, let us consider duration of laminar phases in a course of intermittent dynamics generated by the map with added branch ensuring the presence of reinjection mechanism (13). In the usual Pomeau – Manneville intermittency of type I the average duration of the laminar stages behaves as $\langle t_{lam} \rangle \propto \Delta b^{\nu}$ with $\nu = 0.5$ [Pomeau and Manneville (1980)], [Hirsch *et al.* (1982)], [Hu and Rudnick (1982)]. In presence of the quasiperiodic force the same law is valid in the subcritical region, $\varepsilon < 2$. In the critical case $\varepsilon = 2$ the exponent is distinct. Indeed, as follows from the RG results, to observe increase of a characteristic time scale by factor $\theta = w^{-1} = 1.61803$ we have to decrease a shift of parameter b from the bifurcation threshold by factor $\delta_1 = 3.13427$. As follows, the exponent must be $\nu = \log\theta/\log\delta_1 \cong 0.42123$. Figure 7.26 shows data of numerical experiments with the fractional-linear map. At each fixed ε an average duration of passage through the 'channel' near the formerly existed attractor-repeller pair was computed in dependence on Δb for ensemble of orbits with random initial conditions. Results are plotted in the double logarithmic scale. For particular $\varepsilon = 1.7$ (subcritical) and 2 (critical) the dependencies fit the straight lines of a definite slope, estimated as 0.508 and 0.424, in good agreement with the theory. At subcritical ε slightly less than 2 one can observe a 'crossover' phenomenon: the slope changes from the critical to the subcritical value at some intermediate value of Δb.

In the top panel of Fig.7.27 we reproduce a sketch of the parameter plane near the TF point in the scaling coordinates for the model map (13). Other panels marked (a) and (b) present the bifurcation diagrams and Lyapunov exponent plots corresponding to the paths in the parameter plane designated with respective letters. The point TF is located on a border of stability of a torus-attractor and separates situations of a smooth tori collision and fractal tori collision. Note differences with the TCT point discussed in the previous section. First, there is no a break of the bifurcation border; the point TF is a

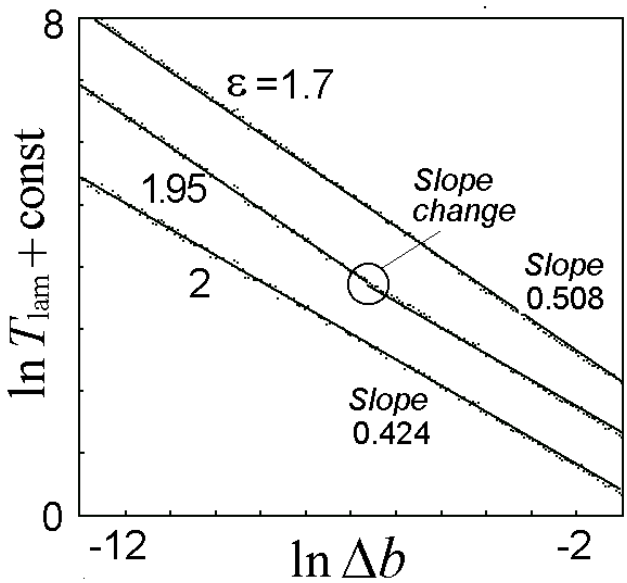

Figure 26: Data of numerical experiments with the fractional-linear map: average duration of passage through the 'channel' versus deflection from the bifurcation threshold for three values of ε in the double logarithmic scale. Observe a 'crossover' phenomenon, the slope change from critical to subcritical value at some intermediate value of Δb for $\varepsilon = 1.95$.

special point of a *smooth* bifurcation curve (in scaling coordinates it looks as a vertical straight line). Second, the fractal tori collision is of a distinct type: the both two partners (a stable and an unstable invariant curve) become fractal at the collision: on each of them narrow sharp 'spikes' are formed; at the collision they touch with these spikes.

A cross of the bifurcation curve gives rise to intermittent dynamics, if a re-injection mechanism is present. At the part of the bifurcation curve corresponding to a smooth tori collision the intermittency is analogous to that studied by Pomeau and Manneville associated with a tangent bifurcation of one-dimensional maps (in particular, the critical indices are the same). At the part of the border corresponding to the fractal tori collision the intermittency gives rise to SNA.

From the point of view of the theory of one-dimensional maps, it is not surprising that the TCT and TF point relate to distinct universality classes: The first occurs in a situation of negative Schwarzian derivative, and the second – of zero Schwarzian derivative. (The Schwarzian derivative for a function $f(x)$ is defined as $S = f'''/f' - \frac{3}{2}(f''/f')^2$, and the main property is that a composition of functions with the same sign of S has the Schwarzian derivative of the same sign [Singer (1978)].)

9 Critical behavior in realistic systems

Since now, in this chapter we dealt with artificial models, the driven one-dimensional maps. However, one can expect that the same types of critical behavior will occur in many realistic systems under quasiperiodic driving, e.g. described by higher dimensional dissipative maps or differential equations. Each type of critical behavior gives rise to a certain universality class. The scaling regularities with definite scaling factors, universal structure of the critical attractor, and universal arrangement of structure of the parameter space near the critical point, with a certain collection of the transition scenarios, should present as the attributes of the universality class. Heuristically, the hypothesis of universality follows from the RG argumentations, in the same spirit as the Feigenbaum universality for classic period doubling: The form of evolution operators for large time intervals is determined by the structure of the RG equation rather than by a concrete original system. However, formally speaking, this assertion needs a rigorous proof, which is nontrivial for systems distinct from the forced one-dimensional maps. Nev-

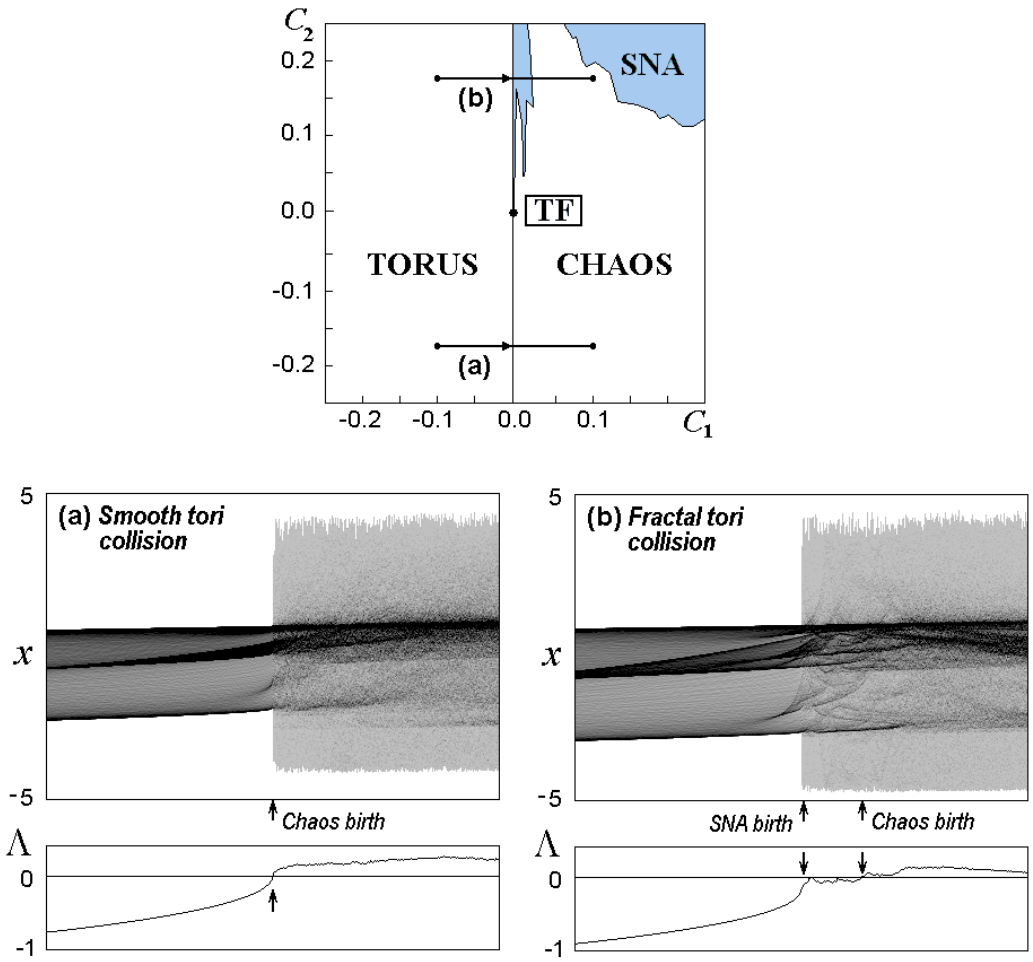

Figure 27: The top panel is a sketch of the parameter plane topography near the TF point in scaling coordinates in a case of presence of the re-injection mechanism. The areas of torus, SNA, and chaos are shown. Panels (a) and (b) present the bifurcation diagrams (x variable versus parameter) and Lyapunov exponent plots along the paths in the parameter plane marked with the respective letters. The path (a) corresponds to collision of smooth stable and unstable tori with their subsequent disappearance and intermittent transition to chaos. On the path (b) the bifurcation consists in a fractal collision of a stable and unstable invariant curves with sharp narrow 'spikes', which appear in a course of approach to the bifurcation

ertheless, we may suggest some qualitative recommendations for a search of the critical points in realistic systems, and present some examples.

Concerning the critical points of TDT and TCT type, it is clear that they may be found is many nonlinear dissipative systems, which demonstrate, as autonomous, the Feigenbaum period-doubling transition to chaos. In presence of the additional periodic force with a frequency in incommensurate (the golden mean) ratio with the characteristic frequency of the system, instead of the period-doubling bifurcations, we will have the torus-doubling bifurcations terminated at some amplitute of the additional force at the TDT points. Instead of the tangent bifurcations we will get the torus collision bifurcation terminated at some amplitude of driving, at the TCT points.

An experimental example has been described in Ref. [Bezruchko *et al.* (2000)]. The underlying system is the driven electronic oscillator, the RL-diode circuit (Fig.7.28). As known since the early 80-th, under increase of the force amplitude of one-frequency driving, this system demonstrates the Feigenbaum period-doubling cascade [Testa *et al.* (1982)]. Now, we may add an additional frequency component to have the golden-mean ratio of this component and the main frequency. Then, on the parameter plane of amplitudes of the two components we expect to observe qualitatively the same picture as in a driven quadratic map: The amplitude of the main driving A_1 at frequency ω_1 is analogous to parameter λ, and the amplitude of the second component A_2 at frequency $\omega_2 = \frac{1}{2}(\sqrt{5}-1)\omega_1$ – to parameter ε.

Observation of phase portraits on the screen of the oscilloscope gave a possibility to find bifurcations of torus doubling. Stroboscopic Poincaré section portrait of attractor could be observed using short-time pulse control of the oscilloscope beam, so that the images of points appeared on the screen following with time interval of $2\pi/\omega_1$. Then, the torus is represented by a smooth closed curve, and the doubled torus – by two smooth closed curves, and so forth. Loss of smoothness of the observed curves, or their smearing, could be associated with the onset of SNA or chaos.

To distinguish more carefully regimes of the smooth torus and of SNA an experimental version of criterion suggested in Chapter 3 was adopted. Namely, using operations of multiplication and division of the basic frequency ω_1, a frequency ratio was selected equal to a rational approximant of the golden mean, namely, 13/21, and presence or absence of bifurcations in the system in dependence on the relative phase between two components of the external driving was checked. The presence of the bifurcations was regarded

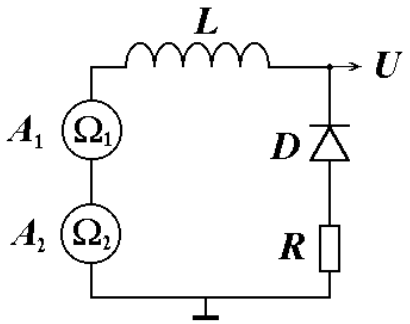

Figure 28: Scheme of the nonlinear electronic circuit under quasiperiodic external driving studied in experiment [Bezruchko *et al.* (2000)]. Two generators produce alternating voltages of amplitudes A_1 and A_2, and frequencies Ω_1 and Ω_2 with a ratio normally equal to the golden mean. Values of A_1 and A_2 are regarded as main control parameters of the system

as indication of the SNA.

In Fig. 7.29 two charts of dynamical regimes are shown, one obtained directly from the experiment and another computed for the forced logistic map. For the first case, the diagram is drawn on the plane of two amplitudes of the external signal (A_1, A_2), for the second case—on the plane (λ, ε). Domains of distinct regimes are indicated by gray tones, and marked with respective inscriptions.

By the analog-digital transformer, the output signal of the system, proportional to voltage on the resistor, could be introduced into a computer and processed. In particular, using data for output voltage with time step equal to one period of the basic frequency $2\pi/\omega_1$, we plot them in coordinates (U_n, U_{n+1}) to obtain the iteration diagrams. In Fig. 7.30 some examples of such diagrams are presented, corresponding to regimes of torus, doubled torus, SNA, and chaos. Both charts in Fig.7.29 look remarkably similar. In particular, one can see there the torus-doubling bifurcation line, which separates regions of torus T1 and doubled torus T2. In experiment, tuning simultaneously two parameters A_2 and A_1, it was sufficiently easy to move along the bifurcation line and find its terminal point, i.e., the TDT critical point. Fig. 7.31 shows how the iteration diagrams of the dynamics evolve in this process. Observe that at the TDT point the attractor accepts a very specific form, similar both in the experimental system and in the quadratic map: It has a fractal-like shape with a break at the leftmost point.

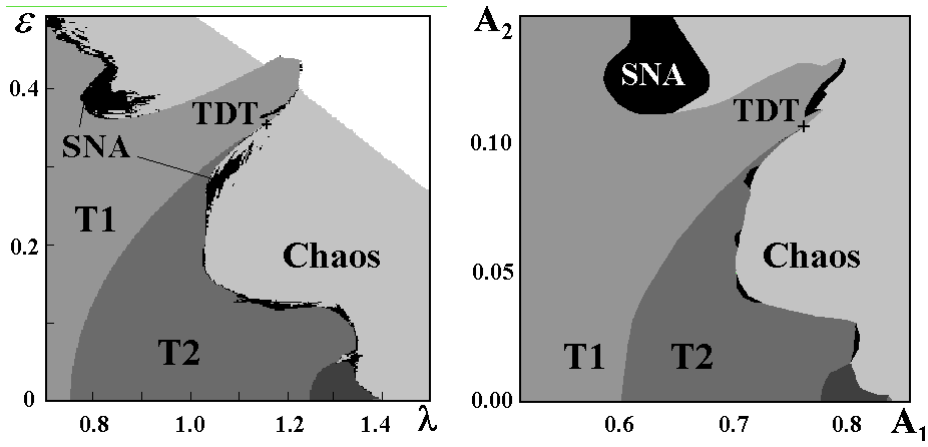

Figure 29: Charts of dynamical regimes obtained in the experiment (a) and computed for the forced quadratic map (b). Areas of existence of smooth tori T1, T2, T4, arisen one from another via the torus-doubling bifurcations, and those of SNA and chaos are marked by respective inscriptions. D is domain of divergence of iterations for the quadratic map. The TDT critical point is indicated by a little cross. For the experimental system amplitudes of two components of the external force, A_1 and A_2 are plotted along the coordinate axes, for the quadratic map coordinates are the control parameter λ and the amplitude of the external force ε

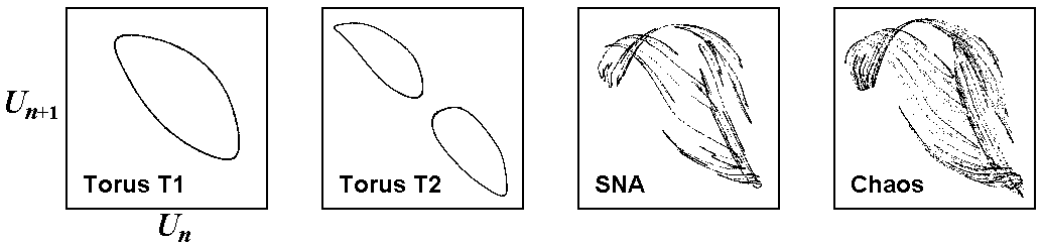

Figure 30: Examples of iteration diagrams obtained by computer processing of data from the experimental system. The diagrams shown relate to torus, double torus, SNA, and chaos, respectively

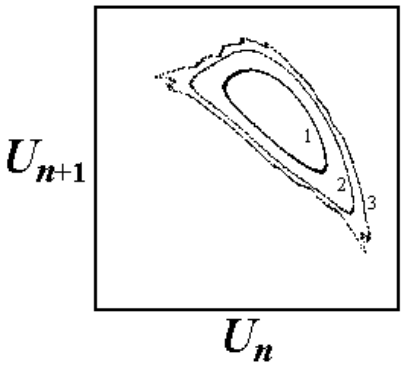

Figure 31: Evolution of the iteration diagram while moving along the torus-doubling bifurcation curve towards the TDT critical point in the experimental system, the quasiperiodically driven RL-diode circuit. Observe a fractal-like shape of the curve representing the critical attractor

Thus, the experiment confirms, at least on a qualitative level, the dynamical behavior associated with existence of the TDT critical point, parameter plane arrangement near this point, and the main peculiarities of the dynamics. Apparently, this experimental system indeed relates to the same universality class as the quasiperiodically forced quadratic map.

Suppose we consider synchronization of a self-oscillating system with periodic pulses near the border of the mode locking. In presence of an additional frequency component, say, modulation of the pulse intensity with incommensurate frequency, the critical situations of TCT and TF type may occur at a sufficient amplitude of the additional frequency component. Indeed, in some approximation the mentioned problem is reduced to the forced circle map. Appearance of the TF critical behavior in subcritical and critical situations, and of TCT in a supercritical situation was mentioned in the previous sections in this Chapter.

The TF critical point is expected to be very typical in many nonlinear dissipative systems, which demonstrate (as autonomous) the saddle-node bifurcation, under quasiperiodic driving. In particular, it was observed in numerics in a model of quasiperiodically forced Josephson junction [Kuznetsov and Neumann (2003)]. The model relates to the high dissipative case and is governed by the ordinary differential equation of the first order,

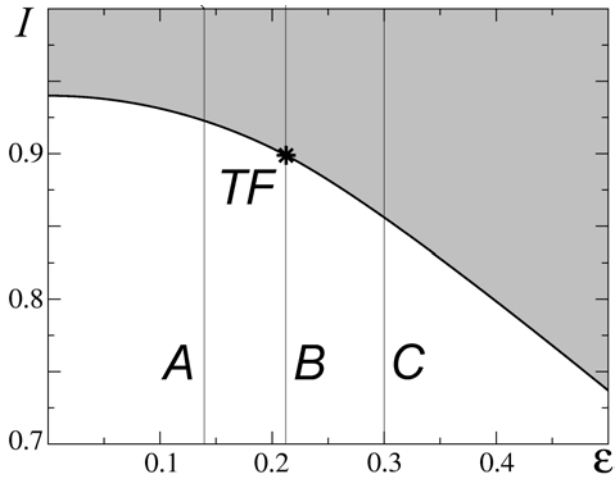

Figure 32: Parameter plane chart of Eq. (77) at $b = 0.5$

represented in dimensionless variables as

$$\dot{x} = -\cos x + I + b\cos t + \varepsilon\cos(wt + \varphi_0), \tag{77}$$

where $x = \phi - \pi/2$, and ϕ is the Josephson phase – the phase difference of the collective wave functions of the Cooper pairs in two pieces of superconductor constituting the junction, I is the constant component of current through the junction, b and ε are amplitudes of two alternate components of the current with frequency ratio $w = \frac{1}{2}(\sqrt{5} - 1)$, φ_0 – a constant initial phase for the second frequency component. (The same equation is appropriate for a mechanical system, a pendulum placed in a vicious medium, with supplied constant angular momentum I and driven by a two-frequency force.)

In Fig.7.32 we reproduce a chart of dynamical regimes, where the bottom (white) area is a region of stability of torus, corresponding to oscillations of the phase φ in a restricted interval. The critical point is placed on the border of this stability region and separates two distinct bifurcation situations, the smooth and fractal tori collision, see illustrations with phase portraits in Fig.7.33. A feature of this system is that chaos does not arise; the smooth tori collision gives birth to a three-frequency quasiperiodic motion. The fractal tori collision gives birth to SNA with a consequent transition to a three-frequency quasiperiodicity.

A convincing demonstration that the criticality is related to the TF universality class is given in Fig.7.34. This is a portrait of the critical attractor

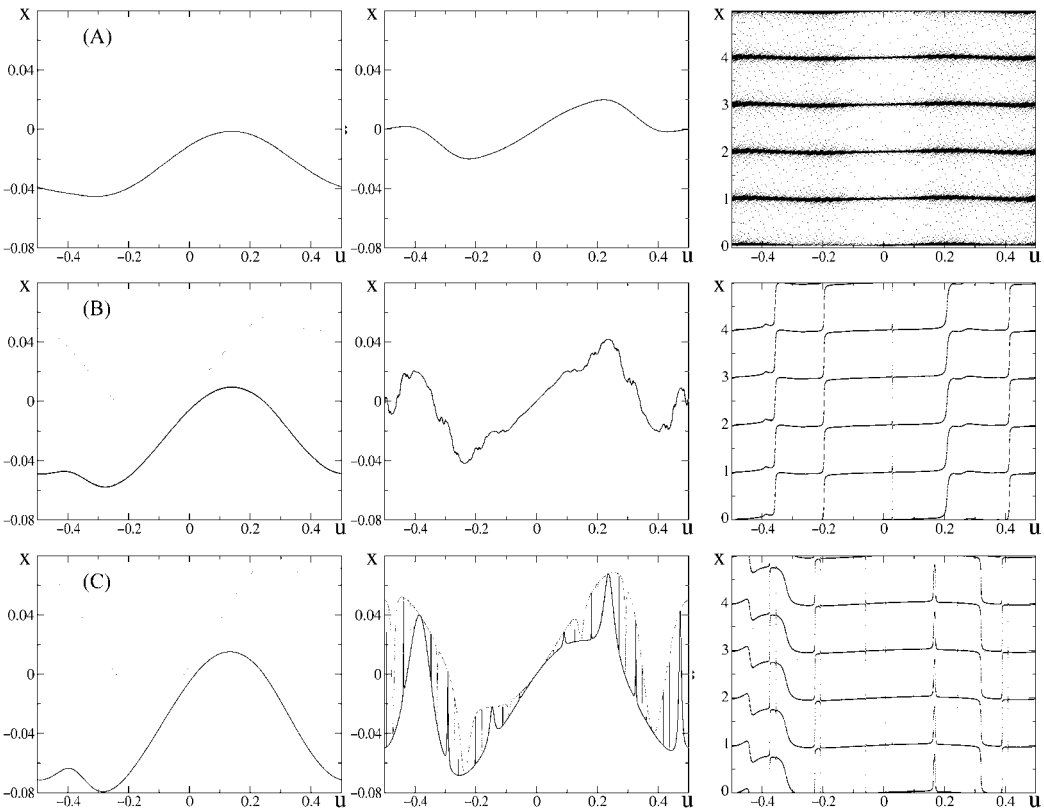

Figure 33: Phase portraits on the plane of variables u and x (panels A, B, C) at representative points of the vertical lines of Fig.32 marked with the respective letters. The phase portraits are plotted with the technique of stroboscopic Poincaré cross-sections $t = 0\,(\mathrm{mod}2\pi)$. Attractors are depicted by solid, and unstable invariant sets by dashed lines: (A) $\varepsilon = 0.14$: $I = 0.9$ (smooth attractor and the unstable invariant curve), $I = 0.922524$ (a single semistable invariant curves), $I = 0.928$ (the attractor is the 3D torus); (B) $\varepsilon = \varepsilon_c = 0.217358$: $I = 0.88$ (smooth attractor and the unstable invariant curve), $I = 0.896801$ (critical attractor, the wrinkled invariant curve), $I = 0.9$ (SNA); (C) $\varepsilon = 0.3$: $I = 0.84$ (smooth attractor and the unstable invariant curve), $I = 0.855914$ (attractor and the unstable invariant set at the fractal collision), $I = 0.87$ (SNA). The right-hand pictures are plotted with variable x defned modulo 5 to show the attractor structure more clearly

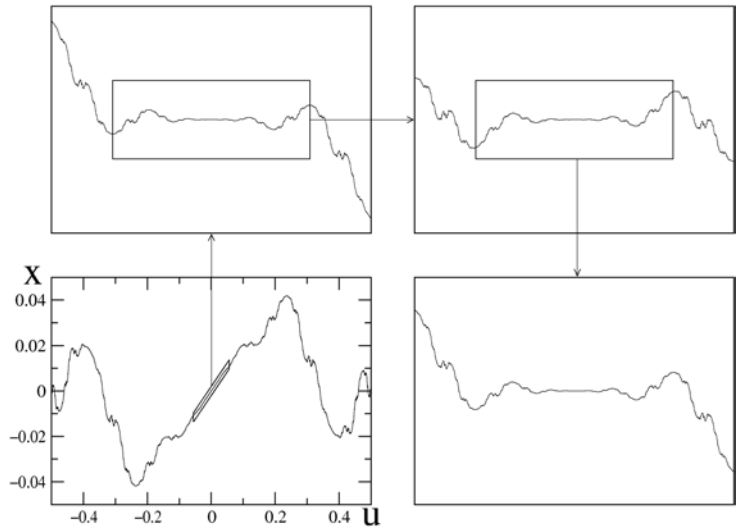

Figure 34: Attractor at the critical point in natural coordinates (u, x) in the Poincaré section and illustration of its self-similarity in scaling coordinates. Factors of magnifcation are $\alpha = 2.89005$ and $\beta = 1/w = 1.618034$ for the vertical and horizontal axes, respectively

in the Poincaré section of the extended phase space by surfaces of constant phase of the first frequency component, $t = 0 \,(\bmod 2\pi)$, on the plane of variables $u = (wt + \varphi_0)/2\pi$ and x. Depicted in properly selected scaling coordinates it demonstrates the self-similarity: The picture reproduces itself under magnification with factors $\alpha = 2.890053$ and $\beta = -w^{-1}$=1.618034 along two coordinate axes. Moreover, the shape of the object is in a good correspondence with that for a model map used for the study of the TF criticality (see Fig. 7.25).

10 Conclusion

Renormalization group analysis, which is of principal significance in the problems concerning the onset of chaos, also appears to be a valuable instrument for a study of the transitions in quasiperiodicqally forced systems involving strange nonchaotic attractors. In this Chapter we have formulated an RG equation that allows analyzing a number of types of critical behavior in quasiperiodically driven systems with the golden-mean frequency ratio.

Due to the fact that the evolution operators for large time intervals are determined by a structure of the RG transformation rather than by a concrete form of the original system, each of the examined types of critical behavior is associated with a certain universality class and may occur in systems of different nature.

An analogous situation takes place in the phase transition theory, where the concepts of RG, universality and scaling are borrowed from. As known, due to universal character of regularities intrinsic to the critical behavior of matter at the phase transitions, it appears productive to use simple models, constructed with a very rough account of the inter-atomic interactions, but representing a universality class of interest (e.g. the models of Ising, Heisenberg etc.). In the same way, in nonlinear dynamics the RG analysis presents a methodological basis for application of simple models, like one-dimensional iterative maps, for establishment and analysis of the fundamental quantitative regularities intrinsic to behavior of nonlinear systems at the border of complex dynamical behavior, like chaos or SNA. Constructing of such models must be recognized as a self-contained significant task of the theory.

The simple models represented by driven one-dimensional maps studied in this Chapter – a pitchfork bifurcation model, quadratic map, circle map, fractional-linear map in vicinities of their critical points are representatives of the respective universality classes, and may serve as samples for consideration of fundamental aspects of the dynamics at the transitions and near them.

We have examine several critical situations intrinsic to the quasiperiodically driven systems with the golden-mean frequency ratio: the blowout transition, the torus doubling terminal point TDT, the torus collision terminal point TCT, the torus fractalization at the intermittency threshold TF. For each of them, a type of the RG equation solution is established, the numerical solution for the functions determining the long-time evolution operators are obtained, the universal constants responsible for the phase space and parameter space scaling properties are accurately estimated. An important general conclusion is that the critical points play a role of, to say, organizing centers for the parameter space arrangement. Any neighborhood of a critical point contains all distinct dynamical regimes relevant for the system. Indeed, due to the scaling properties the picture of dynamical regimes is self-similar, reproducing *ad infinitum* in smaller and smaller scales. In other words, local analysis of the parameter space structure contains in a concentrate form information of possible types of dynamical behavior.

In Fig. 7.34 we reproduce schematic pictures of the universal topogra-

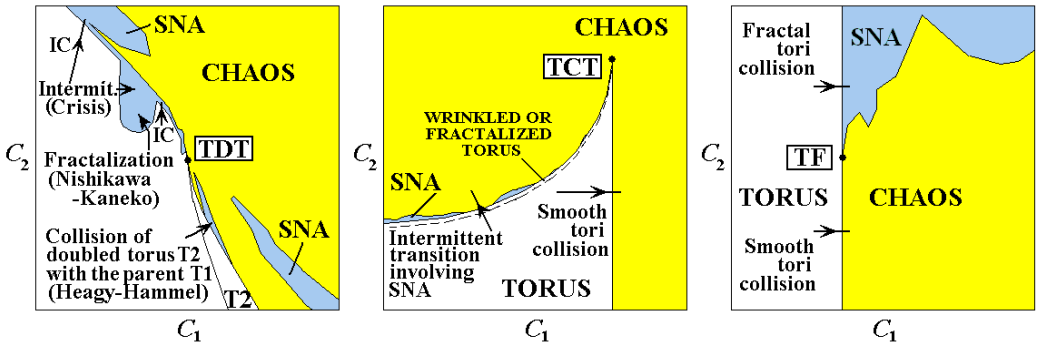

Figure 35: Schematic pictures of the universal topography of the parameter plane near the critical points TDT, TCT, and TF, with indication of the observable transition scenarios. Note that these structures are reproduced in arbitrarily small vicinities of the critical points under appropriate scale change along the vertical and horizontal axes by the universal constants specific for each type of criticality

phy of the parameter plane near the critical points TDT, TCT, and TF. In particular, in a vicinity of the TDT point one can observe scenarios of transitions to SNA and chaos of Heagy and Hammel (birth of SNA due to collision of a doubled torus with an unstable parent torus), intermittent transition, torus fractalization of Kaneko and Nishikawa. At the TCT point two bifurcation borders of the intermittent transitions meet; one corresponds to a birth of intermittent chaos after a smooth tori collision, and another to an intermittent transition involving SNA as an intermediate type of dynamics. The TF point is a special point on the bifurcation border separating two distinct types of the intermittent transition, the smooth tori collision (with transition to chaos, or to a higher dimensional torus), and the birth of SNA via the fractal tori collision.

At the moment, a number of realistic systems demonstrating the mentioned types of critical behavior is rather small, and a search of further examples is an interesting direction of researches. Also, it would be interesting to find out other critical situations, if they do exist. Finally, we emphasize again that our consideration on a basis of the RG approach relate only to the case of the golden-mean quasiperiodicity, and generalizations to other frequency ratios, and for quasiperiodicity with a number of incommensurate frequencies more than two, would be desirable an interesting.

References

[André and Aubry (1980)] André, G. and Aubry, S. (1980). Analyticity breaking and Anderson localization in incommensurate lattices, *Ann. Isr. Phys. Soc.* **3**, pp. 133–164.

[Balescu (1975)] Balescu, R. (1975). Equilibrium and Nonequilibriun Statistical Mechanics, New York, Wiley Publ.

[Bezruchko *et al.* (1997)] Bezruchko, B. P., Kuznetsov, S. P., Pikovsky, A. S., Seleznev, Ye. P. and Feudel, U. (1997). On dynamics of nonlinear systems under external quasi-periodic force near the terminal point of the torus-doubling bifurcation curve, *Applied Nonlinear Dynamics* (Saratov), **5**, 6, pp. 3–19 (in Russian).

[Bezruchko *et al.* (2000)] Bezruchko, B. P., Kuznetsov, S. P. and Seleznev, Ye. P. (2000). Experimental observation of dynamics near the torus-doubling terminal critical point, *Phys. Rev.* **E62**, 6, pp. 7828–7830.

[Cvitanović (1989)] Cvitanović, P., ed. Universality in Chaos, 2nd Edition, Adam Hilger Publ.

[Datta *et al.* (2003)] Datta, S., Sharma, A. and Ramaswamy, R. (2003). Thermodynamics of critical strange nonchaotic attractors, *Phys. Rev.* **E68**, 036104.

[Feigenbaum (1979)] Feigenbaum, M. J. (1979). The universal metric properties of nonlinear transformations, *J. Stat. Phys.* **21**, 6, pp. 669–706.

[Feigenbaum (1983)] Feigenbaum, M. J. (1983). Universal behavior in nonlinear systems. *Physica* **D7**, 1–3, pp. 16–39.

[Feigenbaum *et al.* (1982)] Feigenbaum, M. J., Kadanoff L. P. and Shenker, S. J. (1982). Quasiperiodicity in dissipative systems: A renormalization group analysis. *Physica* **D5**, pp. 370–386.

[Glendinning (2002)] Glendinning, P. (2002). The non-smooth pitchfork bifurcation, http://www.ma.umist.ac.uk/pag/preprints/dspitch.pdf.

[Grebogi *et al.* (1984)] Grebogi, C., Ott, E., Pelikan, S. and Yorke, J. A. (1984). Strange attractors that are not chaotic. *Physica* **D13**, 1–2, pp. 261–268

[Harper, 1955] Harper, P. G. (1955). Single band motion of conduction electrons in a uniform magnetic field. *Proc. Phys. Soc.*, London, Sect. **A68**, pp. 874-878.

[Heagy and Hammel (1994)] Heagy, J. F. and Hammel, S. M. The birth of strange nonchaotic attractors, *Physica* **D70**, 1–2, pp. 140–153.

[Hirsch *et al.* (1982)] Hirsch J. E., Nauenberg, M. and Scalapino, D. J. (1982). Intermittency in the presence of noise: A renormalization group formulation, *Phys. Lett.* **A87**, pp. 391–393.

[Hu and Rudnick (1982)] Hu, B., Rudnik, J. (1982). Exact solution of the Feigenbaum renormalization group equations for intermittency, *Phys. Rev. Lett.* **48**, pp. 1645–1648.

[Ivankov and Kuznetsov (2001)] Ivankov, N. Yu. and Kuznetsov, S. P. (2001). Complex periodic orbits, renormalization and scaling for quasiperiodic golden-mean transition to chaos, *Phys. Rev.* **E63**, 4, 046210.

[Kaneko (1984)] Kaneko, K. (1984) Oscillation and Doubling of Torus, *Progr. Theor. Phys.* **72**, 2, pp. 202–215.

[Ketoja and Satija (1997a)] Ketoja, J. A. and Satija, I. I. (1997a). Harper equation, the dissipative standard map and strange nonchaotic attractors, *Physica* **D109**, pp. 70–80.

[Ketoja and Satija (1997b)] Ketoja, J. A. and Satija, I. I. (1997b). "Critical" phonons of the supercritical Frenkel-Kontorova model: Renormalization bifurcation diagrams, *Physica* **D104**, pp. 239–252.

[Kim *et al.* (2003)] Kim, S.-Y., Lim, W. and Ott, E. (2003). Mechanism for the intermittent route to strange nonchaotic attractors, *Phys. Rev.* **E67**, 056203.

[Kuznetsov (1984)] Kuznetsov, S. P. (1984). Effect of a periodic external perturbation on a system which exhibits an order-chaos transition through period-doubling bifurcations, /it JETP Lett. **39**, 3, pp. 133–136.

[Kuznetsov and Pikovsky (1989)] Kuznetsov, S. P. and Pikovsky, A. S. (1989). Renormalization group for the response function and spectrum of the period-doubling system, *Phys. Lett.* **A140**, 4, pp. 166–172.

[Kuznetsov *et al.* (1997)] Kuznetsov, A. P., Kuznetsov, S. P. and Sataev, I. R. (1997). A variety of period-doubling universality classes in multi-parameter analysis of transition to chaos. *Physica* **D109**, pp. 91–112.

[Kuznetsov *et al.* (1995)] Kunetsov, S. P., Pikovsky, A. S. and Feudel, U. (1995). Birth of a strange nonchaotic attractor: A renormalization group analysis, *Phys. Rev.* **E51**, 3, pp. 1629–1632.

[Kuznetsov *et al.* (1998)] Kunetsov, S. P., Pikovsky, A. S. and Feudel, U. (1998). Renormalization group for scaling at the torus-doubling terminal point, *Phys. Rev.* **E57**, 2, pp. 1585–1590.

[Kuznetsov *et al.* (2000)] Kuznetsov, S. P., Neumann, E., Pikovsky, A. and Sataev, I. R. (2000). Critical point of tori-collision in quasiperiodically forced systems, *Phys. Rev.* **E62**, 2, pp. 1995–2007.

[Kuznetsov (2002)] Kuznetsov, S. P. (2002) Torus fractalization and intermittency, *Phys. Rev.* **E65**, 066209.

[Kuznetsov (2003)] Kuznetsov, S. P. (2003). Generalization of the Feigenbaum-Kadanoff-Shenker renormalization and critical phenomena associated with the golden mean quasiperiodicity. *Syncronization: Theory and applications. NATO Science Series. II. Mathematics, Physics and Chemistry* **109**, Kluwer Academic Publishers, Dordrecht, Boston, London, pp. 79–100.

[Kuznetsov and Neumann (2003)] Kuznetsov, S. P. and Neumann, E. (2003). Torus fractalization and singularities in the current-voltage characteristics for the quasiperiodically forced Josephson junction, *Europhysics Letters* **61**, 1, pp. 20–26.

[Mestel *et al.* (2000)] Mestel, B. D., Osbaldestin, A. H. and Winn, B. (2000). Golden mean renormalization for the Harper equation: The strong coupling fixed point, *J. Math. Phys.*, **41**,12, pp. 8304–8330.

[Negi and Ramaswamy (2001)] Negi, S. S. and Ramaswamy, R. (2001). Critical states and fractal attractors in fractal tongues: Localization in the Harper map, *Phys. Rev.* **E64**, 2001, 045204.

[Nishikawa and Kaneko (1996)] Nishikawa, T. and Kaneko, K. (1996). Fractalization of a torus as a strange nonchaotic attractor, *Phys. Rev.* **E54**, 6, pp. 6114–6124.

[Ostlund *et al.* (1983)] Ostlund, S., Rand, D., Sethna, J. and Siggia, E. D. (1983). Universal properties of the transition from quasi-periodicity to chaos in dissipative systems. *Physica* **D8**, 3, pp. 303–342.

[Pikovsky and Feudel (1995)] Pikovsky, A. S. and Feudel, U. (1995). Characterizing strange nonchaotic attractors, *Chaos* **5**, 1, pp. 253–260.

[Pomeau and Manneville (1980)] Pomeau, Y. and Manneville, P. (1980). Intermittent transition to turbulence in dissipative dynamical systems, *Commun. Math. Phys.* **74**, 2, pp. 189–197.

[Prasad *et al.*(1997)] Prasad, A., Mehra, V. and Ramaswamy, R. (1997). Intermittency Route to Strange Nonchaotic Attractors, *Phys. Rev. Lett.* **79**, 21, pp. 4127–4130.

[Shenker (1982)] Shenker, S. J. (1982). Scaling behavior in a map of a circle onto itself: Empirical results, *Physica* **D5**, pp. 405–411.

[Shirkov *et al* (1988)] Shirkov, D. V., Kazakov, D. I. and Vladimirov, A. A., eds. (1988). Renormalization Group. *Proc. Of Int. Conf., Dubna, 1986*, World Sci. Publ., Singapore.

[Suslov (1982)] Suslov, I. M. Localization in one-dimensional incommensurable systems. *JETP* **83**, 3, pp. 1079–1088 (in Russian).

[Singer (1978)] Singer, D. (1978). Stable orbits and bifurcations of maps of the interval, *SIAM J. Appl. Math.* **35**, 2. pp. 260–267.

[Testa *et al.* (1982)] Testa, J., Perez, J. and Jeffries, C. (1982). Evidence for universal chaotic behavior of a driven nonlinear oscillator, *Phys. Rev. Lett.* **48**, 11, pp. 714–717.

[Vul *et al.* (1984] Vul, E. B., Sinai Y. G. and Khanin, K. M. (1984). Feigenbaum universality and the thermodynamical formalism, *Russ. Math. Surv.* **39**, 3, pp. 1–40.

[Yalçynkaya and Lai (1996)] Yalçynkaya, T. and Lai, Y.-C. (1996). Blowout Bifurcation Route to Strange Nonchaotic Attractors, *Phys. Rev. Lett.* **77**, 25, pp. 5039–5042.